

Hořava Gravity in the Effective Field Theory formalism: from cosmology to observational constraints

Noemi Frusciante^{*1}, Marco Raveri^{†2,3,4}, Daniele Vernieri^{‡1}, Bin Hu^{§5}, and Alessandra Silvestri^{¶5}

¹Sorbonne Universités, UPMC Univ Paris 6 et CNRS, UMR 7095, Institut d’Astrophysique de Paris, GReCO, 98 bis bd Arago, 75014 Paris, France

²SISSA - International School for Advanced Studies, Via Bonomea 265, 34136, Trieste, Italy

³ INFN, Sezione di Trieste, Via Valerio 2, I-34127 Trieste, Italy

⁴ INAF-Osservatorio Astronomico di Trieste, Via G.B. Tiepolo 11, I-34131 Trieste, Italy

⁵Institute Lorentz, Leiden University, PO Box 9506, Leiden 2300 RA, The Netherlands

March 29, 2022

Abstract

We consider Hořava gravity within the framework of the effective field theory (EFT) of dark energy and modified gravity. We work out a complete mapping of the theory into the EFT language for an action including all the operators which are relevant for linear perturbations with up to sixth order spatial derivatives. We then employ an updated version of the EFTCAMB/EFTCosmoMC package to study the cosmology of the low-energy limit of Hořava gravity and place constraints on its parameters using several cosmological data sets. In particular we consider two cases: the first in which the three parameters of the low-energy theory are all varied and a second case that is tuned to evade Post Newtonian constraints, reducing the number of free parameters to two. We employ data sets which include the cosmic microwave background (CMB) temperature-temperature and lensing power spectra by *Planck* 2013, WMAP low- ℓ polarization spectra, the WiggleZ galaxy power spectrum, the local Hubble measurements, Supernovae data from SNLS, SDSS and HST and the baryon acoustic oscillations measurements from BOSS, SDSS and 6dFGS. For both cases we estimate the deviation of the cosmological gravitational constant from the local Newtonian one, getting improved upper bounds with respect to the previous ones from Big Bang Nucleosynthesis data. At the level of the background phenomenology, we find a relevant rescaling of the Hubble rate at all epoch, which has a strong impact on the cosmological observables; at the level of perturbations, we discuss in details all the relevant effects that the modifications of gravity induce, ranging from modifications of the late time Integrated Sachs Wolfe effect, the growth of matter perturbations, gravitational lensing and differences in the B-modes of the CMB. In general the quasi-static approximation is not safe to describe the evolution of perturbations in Hořava gravity. Overall we find that the effects of the modifications induced by the low-energy Hořava gravity action are quite dramatic and current data place tight bounds on the theory parameters.

*E-mail:fruscian@iap.fr

†E-mail:mraveri@sissa.it

‡E-mail:vernieri@iap.fr, **corresponding author**

§E-mail:hu@lorentz.leidenuniv.nl

¶E-mail:silvestri@lorentz.leidenuniv.nl

Contents

1	Introduction	2
2	Theory	3
2.1	Hořava Gravity	3
2.2	Effective Field Theory Framework	4
2.3	Mapping Hořava Gravity into the EFT approach	5
2.4	Degrees of freedom: dynamics and stability	7
3	Hořava Cosmology	10
3.1	Background	10
3.2	Perturbations	12
4	Cosmological constraints	16
4.1	Data sets	16
4.2	H3 case: results	17
4.3	H2 case: results	19
5	Conclusion	20
A	The L_4 and L_6 Lagrangians	22
B	Cosmological Parameters	23

1 Introduction

In their quest to find a quantum theory of gravity that could describe physical phenomena at the Planck scale ($\sim 10^{19}$ GeV/ c^2), relativists have recently started to explore Lorentz violating theories (LV) (see [1] and references therein). Indeed, even though Lorentz invariance (LI) is considered a cornerstone of our knowledge of reality, the challenge presented by physics at Planck energy is forcing us to question also our firmest assumptions. In the cosmological context, LV theories represent interesting candidates for cosmic acceleration, since in their low-energy limit they generally predict a dynamical scalar degree of freedom (DoF) which could provide a source for the late time acceleration, in alternative to the cosmological constant. While the standard model of cosmology, based on the laws of General Relativity (GR), is to date a very good fit to available data, some outstanding theoretical problems related to the cosmological constant have indeed led people to explore alternative theories. To this extent, a wide range of models have been proposed, which either introduce a dynamical dark energy (DE) or modify the laws of gravity on large scales (MG) in order to achieve self accelerating solutions in the presence of negligible matter. All these alternatives generally result in the emergence of new scalar dynamical DoF (see [2, 3, 4] for a comprehensive review), as it is the case with LV theories.

Interestingly, LV theories typically break LI at all scales, and are therefore constrainable with many different measurements and data sets over a vast range of energies. Constraints and measurements on the parameters of a general realistic effective field theory for Lorentz violation [5], usually referred to as the Standard Model Extension [6, 7], support LI with an exquisite accuracy. Furthermore, LI has been tested to high accuracy on solar system scales, and stringent bounds have been placed on the Post Newtonian parameters (PPN), in particular on those corresponding to the preferred frame effects, since such effects are typical of LV theories [8]. Phenomena on astrophysical scales, and in particular tests of gravity in the strong regime, such as those of binary pulsars [9, 10], provide further bounds on LV [8]. On the contrary, the exploration of cosmological bounds on LV theories is still in its infancy [11, 12, 13, 14, 15].

In the present work, we focus on the class of LV theories known as Hořava gravity [16, 17] which modifies the gravitational action by adding higher order spatial derivatives without adding higher order time derivatives, thus modifying the graviton propagator and achieving a power-counting renormalizability. This is possible if one considers that space and time scale differently. Such a prescription is implemented through a breaking of full diffeomorphism invariance, which leads to LV at all scales. The resulting theory propagates a new dynamical scalar DoF, i.e. the spin-0 graviton. As a candidate for quantum gravity, Hořava theory is expected to be renormalizable and also unitary. Nevertheless, at the moment there is no evidence for renormalizability beyond the power-counting arguments.

Hořava gravity shows a rich phenomenology on cosmological scales, e.g. the higher curvature terms in the action lead to a matter bouncing cosmology [18, 19]; it also shows different mechanisms by which it is possible to explain the nearly scale invariant spectrum of cosmological perturbations without introducing an inflationary phase [20, 21, 22, 23], finally, cosmological perturbations at late time have been investigated in refs. [11, 24, 25, 26, 27].

In this paper, we perform a thorough analysis of the cosmology in Hořava gravity by mapping the theory into the framework of Effective Field Theory (EFT) of cosmic acceleration developed in refs. [28, 29, 30, 31, 32, 33, 34], on the line of the EFT of inflation and quintessence [35, 36, 37]. The basic idea of this framework is to construct an effective action with all the operators which are of relevance to study linear cosmological perturbations around a Friedmann-Lemaître-Robertson-Walker (FLRW) background and are invariant under time-dependent spatial diffeomorphisms. Indeed an expanding FLRW background breaks time-dependent diffeomorphism, allowing all these operators to enter the action and, furthermore, to be multiplied by a free function of time [35, 32]. The resulting action encompasses most models of single scalar field DE and MG which have a well defined Jordan frame. In refs. [38, 39, 40, 41], the EFT framework has been implemented in the public Einstein-Boltzmann solver CAMB [42, 43], and the associated Monte Carlo Markov Chain code CosmoMC [44]. The resulting patches, dubbed EFTCAMB/EFTCosmoMC, are now publicly available at <http://wwwhome.lorentz.leidenuniv.nl/~hu/codes/> and represent a powerful package which allows to explore cosmological constraints both in a model independent and model specific way [38]. The original action considered in ref. [29], and implemented in the public version of EFTCAMB, contains all Horndeski and some of the extensions like GLPV [34, 45], but does not have all the operators necessary to study Hořava gravity. The inclusion of Hořava gravity in the context of EFT of DE/MG has been recently considered and investigated in ref. [45]. In this paper, we consider the most general action for Hořava gravity with all the operators with up to sixth order spatial derivatives, which is the minimal prescription to achieve power counting renormalizability. We focus on the part of this action that contributes to linear order in perturbations [46]. For this action we work out a complete mapping to the EFT framework deriving also the generalization of the original EFT action used in refs. [38, 34]. When we compare the predictions of the theory to the observations, we consider only the low-energy operators of Hořava gravity, since those are the relevant ones to describe the large scale cosmology associated to the observables that we employ. We work out the contribution of these operators to the equations of motion for linear scalar and tensor perturbations, implementing them in an updated version of EFTCAMB that will be publicly released in the near future.

The structure of the paper is the following. In section 2, we set up the theoretical background of the paper. In particular, in section 2.1, we introduce Hořava gravity and its main features, while in section 2.2, we summarize the EFT framework and its implementation in EFTCAMB/EFTCosmoMC. In section 2.3 we work out the mapping of Hořava gravity in the EFT language focusing on the low-energy part of the action and leaving the mapping of the high-energy part of the action to appendix A. Finally, in section 2.4, we discuss the requirements that EFTCAMB enforces on the scalar and tensor DoFs to prevent instabilities in the theory. In section 3, we study the cosmology of Hořava gravity, discussing in detail how the model is implemented in EFTCAMB and what are the general effects of the modifications on the background and the perturbations. Finally, in section 4 we explore observational constraints from several combinations of cosmological data sets. To this extent we consider two cases: the low-energy Hořava gravity action which is characterized by three constant parameters; a subcase of the latter, that evades PPN constraints and is characterised by two parameters. We draw our conclusions in section 5, discussing the main results.

2 Theory

In this section we set up the theoretical basis for our analysis. In section 2.1, we introduce the main aspects of Hořava gravity, which is the theory we want to investigate and constrain by using the EFT approach. In section 2.2, we review the EFT framework, discussing its implementation in EFTCAMB, which is the Einstein-Boltzmann solver we use to perform a thorough investigation of the cosmology of the theory. In section 2.3, we work out the mapping of the low-energy Hořava gravity action in terms of the EFT functions. The mapping of the high-energy part of the action is discussed in appendix A. Finally, in section 2.4 we present the full set of equations evolved by EFTCAMB and the conditions that we impose on the tensor and scalar DoFs to ensure that the theory we are considering is viable.

2.1 Hořava Gravity

Hořava gravity has been recently proposed as a candidate for an ultraviolet completion of GR [16, 17]. The basic idea is to modify the graviton propagator by adding to the action higher-order spatial derivatives without adding higher-order time derivatives, in order to avoid the presence of Ostrogradski instabilities [47]. The theory is constructed in such a way to be compatible with a different scaling of space and time, i.e.

$$[dt] = [k]^{-z}, \quad [dx] = [k]^{-1}, \quad (1)$$

where z is a positive integer and k is the momentum. In order to accommodate such a different scaling between space and time, the action of Hořava gravity cannot still be invariant under the full set of diffeomorphisms as in GR, but it can be invariant under the more restricted foliation-preserving diffeomorphisms

$$t \rightarrow \tilde{t}(t), \quad x^i \rightarrow \tilde{x}^i(t, x^i). \quad (2)$$

Therefore, within this approach, space and time are naturally treated on different footing leading to Lorentz violations at all scales. The emergence of LV is reflected in modified dispersion relations for the propagating DoFs. From a practical point of view, the different behavior of space and time is achieved by picking a preferred foliation of spacetime, geometrically described within the Arnowitt-Deser-Misner (ADM) formalism.

It has been shown that the theory is power-counting renormalizable if and only if $z \geq d$, where d indicates the number of spatial dimensions, which means that the action has to contain operators with at least $2d$ spatial derivatives [48, 49]. Hence, in a four-dimensional spacetime, $d = 3$, power-counting renormalizability arguments request at least sixth-order spatial derivatives in the action.

Considering the above arguments, the action of Hořava gravity can be written as follows [46]

$$\mathcal{S}_H = \frac{1}{16\pi G_H} \int d^4x \sqrt{-g} (K_{ij}K^{ij} - \lambda K^2 - 2\xi \bar{\Lambda} + \xi \mathcal{R} + \eta a_i a^i + L_4 + L_6) + S_m[g_{\mu\nu}, \chi_i], \quad (3)$$

where g is the determinant of the metric $g_{\mu\nu}$, \mathcal{R} is the Ricci scalar of the three-dimensional space-like hypersurfaces, K_{ij} is the extrinsic curvature, and K is its trace. $\{\lambda, \xi, \eta\}$ are dimensionless running coupling constants, $\bar{\Lambda}$ is the “bare” cosmological constant, $a_i = \partial_i \ln N$ where as usual N is the lapse function of the ADM metric. L_4 and L_6 denote the Lagrangians associated to the higher-order operators, that contain, respectively, fourth and sixth-order spatial derivatives (see appendix A for the explicit expressions of their parts that contribute to linear order perturbations). These Lagrangians constitute the high-energy (HE) part of the action (3), while the operators preceding them represent the low-energy (LE) limit of the theory and are the ones of relevance on large scale. S_m is the matter action for all matter fields, χ_i . Finally, G_H is the coupling constant which can be expressed as

$$G_H = \xi G \quad (4)$$

where G is the “bare” gravitational constant. As demonstrated in ref. [46], the solution of the static point-like mass in the Newtonian limit gives the relationship between the “bare” gravitational constant (G) and the Newtonian one (G_N), i.e.

$$G = G_N \left(1 - \frac{\eta}{2\xi}\right). \quad (5)$$

Then, the coupling in front of the action reads

$$\frac{1}{16\pi G_H} = \frac{m_0^2}{(2\xi - \eta)}, \quad (6)$$

where $m_0^2 = 1/8\pi G_N$ is the Planck mass defined locally.

Notice that the action of GR is recovered when $\lambda = 1$, $\xi = 1$ and $\eta = 0$, and the higher order operators in L_4 and L_6 are not considered.

The symmetry of the theory allows for a very large number of operators $\sim \mathcal{O}(10^2)$ in L_4 and L_6 . In order to limit the huge proliferation of couplings in the full theory, in the first proposal Hořava imposed some restrictions, i.e. projectability and detailed balance (for the details see refs. [50, 51, 52, 53, 54, 55, 56]). In the following we will not impose any of these limitations to the action (3) and we will consider for L_4 and L_6 all the operators which contribute to the dynamics of linear perturbations [46].

2.2 Effective Field Theory Framework

In the effective field theory approach to DE/MG [28, 29], an action is built in the Jordan frame and unitary gauge by considering the operators which are invariant under time-dependent spatial diffeomorphisms. The additional scalar DoF representing DE/MG is eaten by the metric via a foliation of space-time into space-like hypersurfaces which correspond to a uniform scalar field. At quadratic order, which is sufficient to study the dynamics of linear perturbations, the action reads

$$\begin{aligned} \mathcal{S}_{EFT} = \int d^4x \sqrt{-g} \left\{ \frac{m_0^2}{2} [1 + \Omega(\tau)] R + \Lambda(\tau) - c(\tau) a^2 \delta g^{00} + \frac{M_2^4(\tau)}{2} (a^2 \delta g^{00})^2 - \frac{\bar{M}_1^3(\tau)}{2} a^2 \delta g^{00} \delta K^\mu{}_\mu \right. \\ \left. - \frac{\bar{M}_2^2(\tau)}{2} (\delta K^\mu{}_\mu)^2 - \frac{\bar{M}_3^2(\tau)}{2} \delta K^\mu{}_\nu \delta K^\nu{}_\mu + m_2^2(\tau) (g^{\mu\nu} + n^\mu n^\nu) \partial_\mu (a^2 g^{00}) \partial_\nu (a^2 g^{00}) \right. \\ \left. + \frac{\hat{M}^2(\tau)}{2} a^2 \delta g^{00} \delta \mathcal{R} + \dots \right\} + S_m[g_{\mu\nu}, \chi_m], \quad (7) \end{aligned}$$

where R is the four-dimensional Ricci scalar, δg^{00} , δK^μ_ν , δK^μ_μ and $\delta \mathcal{R}$ are respectively the perturbations of the upper time-time component of the metric, the extrinsic curvature and its trace and the three dimensional spatial Ricci scalar. Finally, S_m is the matter action. Since the choice of the unitary gauge breaks time diffeomorphism invariance, each operator in the action can be multiplied by a time-dependent coefficient; in our convention, $\{\Omega, \Lambda, c, M_2^4, \bar{M}_1^3, \bar{M}_2^2, \bar{M}_3^2, m_2^2, \hat{M}^2\}$ are unknown functions of the conformal time, τ , and we will refer to them as EFT functions. In particular, $\{\Omega, c, \Lambda\}$ are the only functions contributing both to the dynamics of the background and of the perturbations, while the others play a role only at level of perturbations. Let us notice that the above action includes explicitly all the operators that in ref. [29] have been considered to be relevant for linear cosmological perturbations since they can be easily related to some well known DE/MG models such as $f(R)$, quintessence, Horndeski, or because they have been already studied in the EFT of inflation [36, 37, 35]. For such operators the corresponding field equations have been worked out [29, 38]. However, additional second order operators can also be considered, such as $(\delta \mathcal{R})^2$, $\delta \mathcal{R}^i_j \delta \mathcal{R}^j_i$ as well as operators with higher-order spatial derivatives acting on them, [28, 29, 30, 45]. In particular, as we will show in appendix A, additional operators are needed to describe Hořava gravity in the EFT framework (see also [45]).

As mentioned in the Introduction, action (7) allows to describe in a unified language all single scalar field dark energy and modified gravity models which have a well defined Jordan frame. In unitary gauge the extra scalar DoF is hidden inside the metric perturbations, however in order to study the dynamics of linear perturbations and investigate the stability of a given model, it is convenient to make it explicit by means of the Stückelberg technique i.e. performing an infinitesimal coordinate transformation such that $\tau \rightarrow \tau + \pi$, where the new field π is the Stückelberg field which describes the extra propagating DoF. Correspondingly, all the functions of time in action (7) are expanded in Taylor-series and the operators transform accordingly to the tensor transformation laws [28, 29]. Varying the action with respect to the π -field one obtains a dynamical perturbative equation for the extra DoF which allows to control directly the stability of the theory, as discussed at length in ref. [38].

In refs. [38, 39] the effective field theory framework has been implemented into CAMB/CosmoMC [42, 43, 44] creating the EFTCAMB/EFTCosmoMC patches which are publicly available at <http://wwwhome.lorentz.leidenuniv.nl/~hu/codes/> (see ref. [41] for technical details). EFTCAMB evolves the full equations for linear perturbations without relying on any quasi-static (QS) approximation. In addition to the standard matter components (i.e. dark matter, radiation and massless neutrinos), massive neutrinos have also been included [40]. EFTCAMB allows to study perturbations in a model independent way (usually referred to as *pure* EFT mode), investigating the cosmological implications of the different operators in action (7). It can also be used to study the exact dynamics for specific models, after the mapping of the given model into the EFT language has been worked out (usually referred to as *mapping* mode). In the latter case one can treat the background via a designer approach, i.e. fixing the expansion history and reconstructing the specific model in terms of EFT functions; or one can solve the full background equations of the chosen theory. We refer to the latter as the *full mapping* case. Furthermore, the code has a powerful built-in module that investigates whether a chosen model is viable, through a set of general conditions of mathematical and physical stability. In particular, the physical requirements include the avoidance of ghost and gradient instabilities for both the scalar and the tensor DoFs. The stability requirements are translated into *viability priors* on the parameter space when using EFTCosmoMC to interface EFTCAMB with cosmological data, and they can sometimes dominate over the constraining power of data [39]. In this paper we will study the case of Hořava gravity, first describing how it can be cast into EFTCAMB via a full mapping, then exploring the effects of the stability conditions on its parameter space and finally deriving constraints from different combinations of cosmological data sets.

2.3 Mapping Hořava Gravity into the EFT approach

In this section we will work out explicitly the mapping of the low-energy (LE) part of action (3) into the EFT formalism described in the previous section. This is the part of the action for which we will explore cosmological constraints. We show the mapping for the high-energy (HE) part (L_4 and L_6) in the appendix A.

We use the following conventions: $(-, +, +, +)$ for the signature of the metric $g_{\mu\nu}$; the background is considered FLRW with $\kappa = 0$; dots are derivatives w.r.t. conformal time, τ and $\mathcal{H} \equiv \dot{a}/a$ is the Hubble rate; we will use the superscript (0) for the background quantities; finally we define a time-like unit vector, n_μ as

$$n_\mu = \frac{\partial_\mu t}{\sqrt{-g^{\alpha\beta} \partial_\alpha t \partial_\beta t}}, \quad \text{with} \quad n_\mu n^\mu = -1, \quad (8)$$

which corresponds to the convention that we use for the normal vector to the uniform-field hypersurfaces in the EFT construction of the action (7) [29, 38]. In conformal time and at second order in perturbations, one has

$$n_\mu = \delta_\mu^0 \left(1 + \frac{1}{2} a^2 \delta g^{00} + \frac{3}{8} (a^2 \delta g^{00})^2 \right), \quad (9)$$

$$n^\mu = g^{0\mu} \left(1 + \frac{1}{2} a^2 \delta g^{00} + \frac{3}{8} (a^2 \delta g^{00})^2 \right). \quad (10)$$

In the following, these relations will be often employed.

Let us first recall the low-energy action, which can be rewritten as:

$$\begin{aligned} \mathcal{S}_{H,LE} &= \frac{m_0^2}{(2\xi - \eta)} \int d^4x \sqrt{-g} (K_{ij} K^{ij} - \lambda K^2 + \xi \mathcal{R} - 2\xi \bar{\Lambda} + \eta a_i a^i) \\ &= \frac{m_0^2}{(2\xi - \eta)} \int d^4x \sqrt{-g} (\xi R + (1 - \xi) K^{ij} K_{ij} + (\xi - \lambda) K^2 - 2\xi \bar{\Lambda} + \eta a_i a^i) + \text{boundary terms}, \end{aligned} \quad (11)$$

where the second line has been obtained by using the Gauss-Codazzi relation [57].

In the following, we show how to rewrite every single term of the above action in the EFT formalism described by the action (7), providing the mapping of the Hořava gravity parameters into the EFT functions.

- $\frac{m_0^2 \xi}{(2\xi - \eta)} (R - 2\bar{\Lambda})$

Comparing the above expression with the EFT action (7), it is straightforward to deduce that these two terms contribute to the following EFT functions

$$(1 + \Omega) = \frac{2\xi}{(2\xi - \eta)}, \quad \Lambda = -2 \frac{m_0^2 \xi}{(2\xi - \eta)} \bar{\Lambda}. \quad (12)$$

- $\frac{m_0^2}{(2\xi - \eta)} (\xi - \lambda) K^2$

In order to identify the relation between the EFT functions and the Hořava gravity parameters we have to expand K^2 up to second order in perturbations as

$$K^2 = 2K^{(0)}K + (\delta K)^2 - K^{(0)2}, \quad (13)$$

by using $K = K^{(0)} + \delta K$. Comparing the above relation with the action (7), it is straightforward to see that the last term gives contribution to $\Lambda(\tau)$ and the second one to $\bar{M}_2^2(\tau)$. The first term can be computed as follows [28]

$$\begin{aligned} \int d^4x \sqrt{-g} 2K^{(0)}K &= 2 \int d^4x \sqrt{-g} K^{(0)} (\nabla_\mu n^\mu) = -2 \int d^4x \sqrt{-g} \nabla_\mu K^{(0)} n^\mu \\ &= 2 \int d^4x \sqrt{-g} \frac{\dot{K}^{(0)}}{a} \left[1 - \frac{1}{2} (a^2 \delta g^{00}) - \frac{1}{8} (a^2 \delta g^{00})^2 \right], \end{aligned} \quad (14)$$

where we have integrated by parts the second line and we have used eq. (10). The last line will give respectively its contribution to $\Lambda(\tau)$, $c(\tau)$ and $M_2^4(\tau)$. Then summarizing, the corresponding contributions to the EFT functions from the K^2 term are

$$\begin{aligned} \Lambda(\tau) &= -\frac{m_0^2 (\xi - \lambda)}{(2\xi - \eta)} \left(K^{(0)2} - 2 \frac{\dot{K}^{(0)}}{a} \right), \quad c(\tau) = \frac{m_0^2 (\xi - \lambda)}{(2\xi - \eta)} \frac{\dot{K}^{(0)}}{a}, \\ M_2^4(\tau) &= -\frac{m_0^2 (\xi - \lambda)}{2(2\xi - \eta)} \frac{\dot{K}^{(0)}}{a}, \quad \bar{M}_2^2(\tau) = -\frac{2m_0^2}{(2\xi - \eta)} (\xi - \lambda). \end{aligned} \quad (15)$$

- $\frac{m_0^2 (1 - \xi)}{(2\xi - \eta)} K_{ij} K^{ij}$

As before, we can expand up to second order in perturbations the above operator and it can be written as

$$K_{ij} K^{ij} = 2K_{ij}^{(0)} \delta K^{ij} + K^{ij(0)} K_{ij}^{(0)} + \delta K_{ij} \delta K^{ij}, \quad (16)$$

where we have used the spatial metric to raise the indices and the extrinsic curvature has been decomposed into its background and first order perturbation parts, i.e. $K_{ij} = K_{ij}^{(0)} + \delta K_{ij}$. Moreover, the first term can be written as

$$2K_{ij}^{(0)} \delta K^{ij} = -2 \frac{\mathcal{H}}{a} \delta K = -2 \frac{\mathcal{H}}{a^2} (aK + 3\mathcal{H}), \quad (17)$$

where the term proportional to K can be treated as in eq. (14). Finally, in terms of the EFT functions this operator can be written as

$$\begin{aligned}\Lambda(\tau) &= -\frac{m_0^2(1-\xi)}{(2\xi-\eta)} \left[K^{ij(0)} K_{ij}^{(0)} + \frac{2}{a^2} (\dot{\mathcal{H}} - \mathcal{H}^2) \right], & c(\tau) &= -\frac{m_0^2(1-\xi)}{(2\xi-\eta)a^2} (\dot{\mathcal{H}} - \mathcal{H}^2) \\ M_2^4(\tau) &= \frac{m_0^2(1-\xi)}{2a^2(2\xi-\eta)} (\dot{\mathcal{H}} - \mathcal{H}^2), & \bar{M}_3^2 &= -2\frac{m_0^2(1-\xi)}{(2\xi-\eta)}.\end{aligned}\quad (18)$$

- $\frac{m_0^2}{(2\xi-\eta)} \eta a_i a^i$

Let us first write explicitly a_i in terms of perturbations up to second order

$$a_i = \frac{\partial_i N}{N} = -\frac{1}{2} \frac{\partial_i (a^2 g^{00})}{a^2 g^{00}} = \frac{1}{2} \partial_i \delta (a^2 g^{00}) + \mathcal{O}(2), \quad (19)$$

where in the last equality we have used $a^2 g^{00} = -1 + a^2 \delta g^{00}$ and then we have expanded in Taylor series. Then we get

$$\frac{m_0^2}{(2\xi-\eta)} \eta a_i a^i = \frac{m_0^2}{4(2\xi-\eta)} \eta \frac{\tilde{g}^{ij}}{a^2} \partial_i (a^2 \delta g^{00}) \partial_j (a^2 \delta g^{00}), \quad (20)$$

where \tilde{g}^{ij} is the background value of the spatial metric. In the EFT language the above expression corresponds to

$$m_2^2 = \frac{m_0^2 \eta}{4(2\xi-\eta)}. \quad (21)$$

Summarizing, we can map the low-energy action (11) of Hořava gravity in the EFT language at the basis of EFTCAMB as follows:

$$\begin{aligned}(1 + \Omega) &= \frac{2\xi}{(2\xi-\eta)}, \\ c(\tau) &= -\frac{m_0^2}{a^2(2\xi-\eta)} (1 + 2\xi - 3\lambda) (\dot{\mathcal{H}} - \mathcal{H}^2), \\ \Lambda(\tau) &= \frac{2m_0^2}{(2\xi-\eta)} \left[-\xi \bar{\Lambda} - (1 - 3\lambda + 2\xi) \left(\frac{\mathcal{H}^2}{2a^2} + \frac{\dot{\mathcal{H}}}{a^2} \right) \right], \\ \bar{M}_3^2 &= -\frac{2m_0^2}{(2\xi-\eta)} (1 - \xi), \\ \bar{M}_2^2 &= -2\frac{m_0^2}{(2\xi-\eta)} (\xi - \lambda), \\ m_2^2 &= \frac{m_0^2 \eta}{4(2\xi-\eta)}, \\ M_2^4(\tau) &= \frac{m_0^2}{2a^2(2\xi-\eta)} (1 + 2\xi - 3\lambda) (\dot{\mathcal{H}} - \mathcal{H}^2), \\ \bar{M}_1^3 &= \hat{M}^2 = 0,\end{aligned}\quad (22)$$

where we have explicitly written the value of the extrinsic curvature and its trace on a flat FLRW background¹. The mapping of the high-energy part of the action can be found in appendix A.

2.4 Degrees of freedom: dynamics and stability

After the full diffeomorphism invariance is restored by means of the Stückelberg mechanism, at the level of perturbations we have a dynamical equation for the scalar DoF represented by the Stückelberg field π . In the case of the low-energy limit of Hořava gravity that we are considering, this equation reads

$$\eta \ddot{\pi} + 2\eta \mathcal{H} \dot{\pi} + \left[(3\lambda - 2\xi - 1)(\mathcal{H}^2 - \dot{\mathcal{H}}) + \eta(\mathcal{H}^2 + \dot{\mathcal{H}}) \right] \pi + k^2 \xi (\lambda - 1) \pi + \xi (\lambda - 1) k \mathcal{Z} + \frac{(\xi - 1)(2\xi - \eta)}{2k} \left[\frac{a^2 (\rho_i + p_i)}{m_0^2} v_i \right] = 0, \quad (23)$$

¹For the low-energy action it is possible to obtain part of the mapping by following the method in ref. [30]. However, one has to consider that our formalism and notation differ from the one in ref. [30] because we are using conformal time, a different signature for the normal unit vector, a different notation for the EFT functions and one more operator is included in our low-energy action: $a_\mu a^\mu$.

where \mathcal{Z} is the standard CAMB variable [42, 43, 44] ρ_i, p_i are the background density and pressure of matter components, and v_i is the velocity perturbation of matter components. The above equation is coupled with the following perturbative field equations:

- time-time (**t**) field equation

$$2\mathcal{H} [k^2\pi(\eta - 3\lambda + 2\xi + 1) + (1 - 3\lambda)k\mathcal{Z}] + 2k^2(2\xi\bar{\eta} + \eta\dot{\pi}) + a^2\frac{2\xi - \eta}{m_0^2}\delta\rho_m = 0, \quad (24)$$

- space-space (**s**) field equation

$$-4\mathcal{H} [k^2(3\lambda - 2\xi - 1)\pi + (3\lambda - 1)k\mathcal{Z}] + (1 - 3\lambda)\ddot{h} + 4k^2\xi\bar{\eta} + 2k^2(-3\lambda + 2\xi + 1)\dot{\pi} + 3a^2\frac{(\eta - 2\xi)}{m_0^2}\delta P_m = 0, \quad (25)$$

where $h, \bar{\eta}$ are the usual scalar perturbations of the metric in synchronous gauge (notice that we have added a bar to the standard metric perturbation in order to do not confuse it with the Hořava gravity parameter, η). EFTCAMB evolves the above set of coupled differential equations along with the usual matter perturbation equations. Let us notice that by using the mapping (22) worked out in the previous section, it is straightforward to deduce the above equations following the general prescription in ref. [38].

We shall now determine the dispersion relation of the scalar DoF, computing the determinant of the matrix of the coupled system eqs. (23)- (25). Since the number counting of dynamical DoFs will not be changed by neglecting the couplings with standard matter species, for simplicity, for the purpose of this calculation we neglect them. After taking the Fourier transform $\partial_\tau \rightarrow -i\omega$, we can rewrite the system (23)- (25) in the following matrix form:

$$\begin{pmatrix} \gamma_{\pi\pi} & \gamma_{\pi h} & \gamma_{\pi\bar{\eta}} \\ \gamma_{s\pi} & \gamma_{sh} & \gamma_{s\bar{\eta}} \\ \gamma_{t\pi} & \gamma_{th} & \gamma_{t\bar{\eta}} \end{pmatrix} \begin{pmatrix} \pi \\ h \\ \bar{\eta} \end{pmatrix} = 0, \quad (26)$$

where the term γ_{ab} with $a, b = \{\pi, h, \bar{\eta}\}$ corresponds to the coefficient of b in equation a and they can be easily deduced from the above equations. Finally we set the determinant to zero and get

$$k^4\omega(\omega + i\mathcal{H}) \left[\omega^2 + i2\mathcal{H}\omega - \frac{(\lambda - 1)\xi(2\xi - \eta)}{\eta(3\lambda - 1)}k^2 - \frac{\xi}{\eta} \left((\dot{\mathcal{H}} - \mathcal{H}^2)(\eta - 3\lambda + 2\xi + 1) + (6\lambda - 4\xi - 2)\mathcal{H}^2 \right) \right] = 0, \quad (27)$$

which can be written in a compact form as

$$k^4\omega \left(\omega + i\frac{\alpha}{2} \right) [\omega^2 + i\alpha\omega - k^2c_s^2 + \beta] = 0. \quad (28)$$

From the above equation we deduce that only one extra dynamical DoF exists, which corresponds to the scalar graviton (π field in EFT language), as expected. Furthermore, one can identify the terms in the squared bracket as follows: α is a friction term, β is the dispersion coefficient and c_s^2 can be identified with the canonical speed of sound defined in vacuum, when no friction or dispersive terms are present. Let us notice that both the friction and dispersive terms are related to the nature of the dark energy component through the dependence of the Hubble rate on the latter (38). The procedure to compute the dispersion relation (27) follows the one in ref. [29], but here we include also friction and dispersive terms.

In order to ensure that a given theory is viable, we enforce a set of physical and mathematical viability conditions. The mathematical conditions prevent exponential instabilities from showing up in the solution of the π -field equation, and the physical ones correspond to the absence of ghosts and gradient instabilities for both scalar and tensor modes. In particular, in our analysis of Hořava gravity, for the scalar DoF they correspond to

$$\frac{\eta}{2\xi - \eta} > 0, \quad \frac{\xi(2\xi - \eta)(\lambda - 1)}{\eta(3\lambda - 1)} > 0, \quad (29)$$

where the first condition corresponds to a positive kinetic term, while the second one ensures that the speed of sound is positive.

Additional conditions to be imposed comes from the equation for the propagation of tensor modes h_{ij} ,

$$A_T(\tau)\ddot{h}_{ij} + B_T(\tau)\dot{h}_{ij} + D_T(\tau)k^2h_{ij} + E_{Tij} = 0. \quad (30)$$

where δT_{ij} generally contains the matter contributions coming from the neutrino and photon components and, for Hořava gravity, the remaining coefficients read:

$$A_T = \frac{2}{2\xi - \eta}, \quad B_T = \frac{4\mathcal{H}}{2\xi - \eta}, \quad (31)$$

$$D_T = \frac{2\xi}{2\xi - \eta}, \quad E_{Tij} = \frac{a^2}{m_0^2} \delta T_{ij}. \quad (32)$$

The viability conditions require $A_T > 0$ and $D_T > 0$ to prevent respectively a tensorial ghost and gradient instabilities [41].

It is easy to show that the above conditions translate into the following constraints on the parameters of Hořava gravity:

$$0 < \eta < 2\xi, \quad \lambda > 1 \quad \text{or} \quad \lambda < \frac{1}{3}, \quad (33)$$

which are compatible with the viable regions identified around a Minkowski background [46]. In the following we will not explore the $\lambda < 1/3$ branch since along it the cosmological gravitational constant on the FLRW background becomes unacceptably negative [58, 59] and the branch does not have a continuous limit to GR. The conditions that we have discussed are naturally handled by EFTCAMB/EFTCosmoMC in the form of *viability priors* that are automatically enforced when the parameter space is being sampled.

Besides the above theoretical viability conditions, there are observational constraints on the Hořava gravity parameters coming from existing data. In particular:

- Big Bang Nucleosynthesis (BBN) constraints [11], which set an upper bound on $|G_{cosmo}/G_N - 1| < 0.38$ (99.7% C.L.)², where G_{cosmo} is the cosmological gravitational constant as defined in section 3.1;
- Solar system constraints, where the parametrized post Newtonian parameters (PPN) are bounded to be³:

$$\alpha_1 < 3.0 \cdot 10^{-4} \text{ (99.7\%C.L.)}, \quad \alpha_2 < 7.0 \cdot 10^{-7} \text{ (99.7\%C.L.)}. \quad (34)$$

where α_1 and α_2 are two of the parameters appearing in the PPN expansion of the metric around Minkowski spacetime, more precisely those associated with the preferred frame effects [8, 60]. Here we consider only these two parameters since they are the only ones of relevance for constraining LV. It has been shown in refs. [61, 62, 63], that the PPN parameters for the low-energy action of Hořava gravity, read

$$\alpha_1 = 4(2\xi - \eta - 2), \quad \alpha_2 = -\frac{(\eta - 2\xi + 2)(\eta(2\lambda - 1) + \lambda(3 - 4\xi) + 2\xi - 1)}{(\lambda - 1)(\eta - 2\xi)}. \quad (35)$$

It is easy to show that combining the above relations, the above mentioned PPN bounds result in a direct constraint on λ that reads:

$$\log_{10}(\lambda - 1) < -4.1 \text{ (99.7\%C.L.)}, \quad (36)$$

while the bound on α_1 provides a degenerate constraint on the other two parameters $\{\xi, \eta\}$.

- Čerenkov constraints from the observation of high-energy cosmic rays [64] are usually imposed as a lower bound on the propagation speed of the scalar DoF and the propagation speed of tensor modes. However, since these bounds have not been worked out for Hořava gravity we will not impose them.

For the present analysis we consider two specific cases of Hořava gravity:

1. Hořava 3, hereafter H3, where we vary all three parameters $\{\lambda, \eta, \xi\}$ appearing in the low-energy Hořava gravity action;
2. Hořava 2, hereafter H2, where we choose the theory parameters in order to evade the PPN constraints (35) by setting exactly $\alpha_1 = \alpha_2 = 0$. This implies:

$$\eta = 2\xi - 2, \quad (37)$$

so that the number of free parameters reduce to two, $\{\lambda, \eta\}$. This case has the quality of systematically evading solar system PPN constraints, meaning that it is not possible to build a local experiment, with arbitrary precision, to distinguish it from GR. Therefore it can only be constrained with cosmological observations.

²The original bound in ref. [11] is reported at 68% C.L. and we convert it to 99.7% C.L. by assuming a Gaussian posterior distribution of $G_{cosmo}/G_N - 1$.

³The original bounds in ref. [60] (and references therein) are reported at 90% C.L. and we convert it to 99.7% C.L. by assuming a Gaussian posterior distribution of the relevant parameters.

For both cases we impose the physical and mathematical viability conditions in the form of *viability priors* as discussed in ref. [39]. The portion of the parameter space excluded by the *viability priors* can be seen as a dark grey contour in figure 6 for the H3 case and in figure 7 for the H2 case. For both cases we also derive the bounds on $G_{\text{cosmo}}/G_N - 1$ and for the H3 case we provide cosmological bounds on the PPN parameters. These results are shown and discussed in detail in section 4.

3 Hořava Cosmology

In this section we highlight the cosmological implications of the low-energy Hořava gravity cases, H2 and H3, previously introduced. In section 3.1 we discuss the changes that Hořava gravity induces at the level of the cosmological background, while in section 3.2 we elaborate on the effects that are displayed by the theory at the level of perturbations by means of two examples.

3.1 Background

The first step toward testing a theory against cosmological observations, is to investigate the behaviour of its cosmological background. In this section, we discuss the background evolution equation for Hořava gravity, its implementation in EFTCAMB, and review the definitions that we adopt for the cosmological parameters.

The Hořava gravity field equations for a flat FLRW background read:

$$\frac{3\lambda - 1}{2} \mathcal{H}^2 = \frac{8\pi G_N (2\xi - \eta)}{6} a^2 \sum_i \rho_i + \xi \frac{\bar{\Lambda}}{3} a^2, \quad (38)$$

$$-\frac{3\lambda - 1}{2} \left[\dot{\mathcal{H}} + \frac{1}{2} \mathcal{H}^2 \right] = -\frac{\xi \bar{\Lambda}}{2} a^2 + 4\pi G_N \frac{(2\xi - \eta)}{2} a^2 \sum_i p_i, \quad (39)$$

where ρ_i and p_i are respectively the density and the pressure of the matter fluid components, i.e. baryons and dark matter (m), radiation and massless neutrino (r) and massive neutrinos (ν). In this work we consider that all massive neutrino species have the same mass and we set the sum of their masses to be 0.06 eV. In addition to the Friedmann equations, we have the standard continuity equations for matter and radiation:

$$\dot{\rho}_i + 3\mathcal{H}(1 + w_i)\rho_i = 0, \quad (40)$$

while for massive neutrinos we refer the reader to ref. [40] for a detailed discussion.

Starting from the Friedmann eq. (38), we can define the cosmological gravitational constant as:

$$G_{\text{cosmo}} = \frac{(2\xi - \eta)}{3\lambda - 1} G_N, \quad (41)$$

where it is clear that G_{cosmo} differs from G_N , which is obtained with local experiments, as already pointed out in ref. [46]. This definition allows us to write the Friedmann equation (38) in another way:

$$\mathcal{H}^2 = 8\pi G_{\text{cosmo}} a^2 \left(\frac{\sum_i \rho_i}{3} + \frac{1}{8\pi G_N} \frac{2\xi}{2\xi - \eta} \frac{\bar{\Lambda}}{3} \right). \quad (42)$$

From this equation it is straightforward to see that in general, once the theory parameters have been properly set, the modification that Hořava gravity induces at the level of the background is a global rescaling of \mathcal{H} [15].

In order to properly identify the parameters that we should fit to data, we have to pay special attention to the working definition of all the relevant quantities. In particular in the definition of the relative density abundance. For the matter fields, we define $\Omega_i(a)$ in terms of the locally measured gravitational constant, G_N , and the present time Hubble parameter, H_0 . We then derive the abundance of the effective dark energy, describing the modifications to the Friedmann equations, by means of the flatness condition, i.e. $\sum_i \Omega_i(a) + \Omega_{DE}(a) = 1$. To this extent, we rewrite the Friedmann eq. (38) as

$$\mathcal{H}^2 = 8\pi G_N \frac{\sum_i \rho_i}{3} a^2 + \frac{2\xi}{2\xi - \eta} \frac{\bar{\Lambda}}{3} a^2 + \left(1 - \frac{3\lambda - 1}{2\xi - \eta} \right) \mathcal{H}^2, \quad (43)$$

so that it is straightforward to identify

$$\begin{aligned} \Omega_i(a) &= 8\pi G_N \frac{\rho_i}{3} \frac{a^2}{\mathcal{H}^2}, \\ \Omega_{DE}(a) &= \frac{2\xi}{2\xi - \eta} \frac{\bar{\Lambda}}{3} \frac{a^2}{\mathcal{H}^2} + 1 - \frac{3\lambda - 1}{2\xi - \eta}. \end{aligned} \quad (44)$$

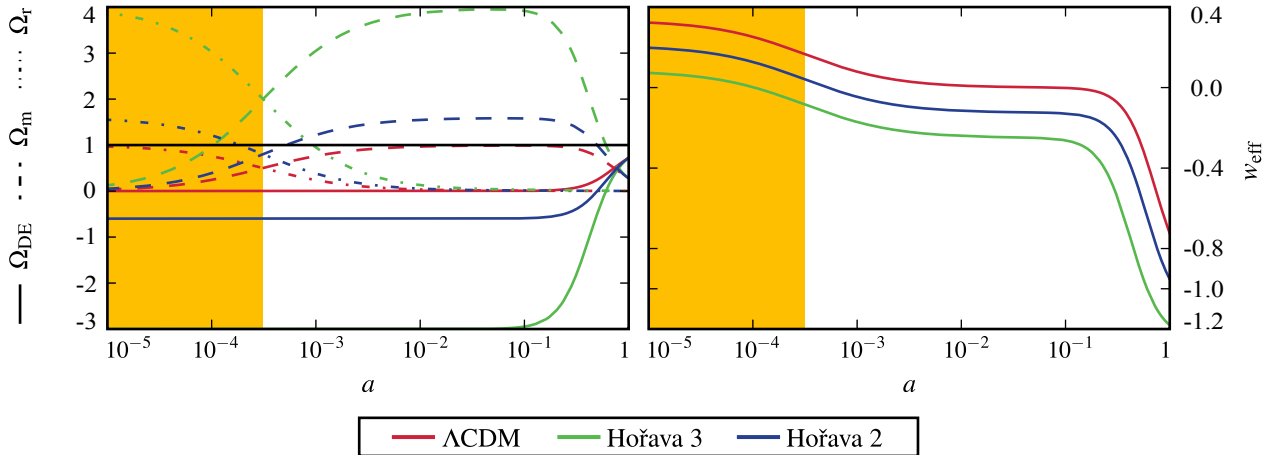


Figure 1: The left panel shows the evolution of the densities parameters for baryons and dark matter (m, dashed line), radiation, neutrino and massive neutrinos (r, dot dashed line) and dark energy (DE, solid line). The right panel shows the behaviour of the effective equation of state. In both panels different colours corresponds to different cases as shown in legend. The yellow area highlights the radiation dominated era. For this figure the standard cosmological parameters are chosen to be $\Omega_b^0 h^2 = 0.0226$, $\Omega_c^0 h^2 = 0.112$, $\Omega_\nu^0 h^2 = 0.00064$ and $H_0 = 70$ Km/s/Mpc. In the H3 case the Hořava gravity parameters are $\lambda = 1.4$, $\xi = 0.9$, $\eta = 1.0$ while in the H2 case they are fixed to $\lambda = 1.4$, $\eta = 1.0$.

At present time ($a_0 = 1$), we can immediately see that $\Omega_{DE}^0 = 1 - \sum_i \Omega_i^0$ with:

$$\Omega_{DE}^0 = \frac{2\xi}{2\xi - \eta} \frac{\bar{\Lambda}}{3H_0^2} + 1 - \frac{3\lambda - 1}{2\xi - \eta}. \quad (45)$$

This allows us to rewrite the Friedmann eq. (38) in terms of the parameters that we are going to sample as:

$$\mathcal{H}^2 = \frac{(2\xi - \eta)}{3\lambda - 1} a^2 H_0^2 \left[\frac{\Omega_m^0}{a^3} + \frac{\Omega_r^0}{a^4} + \rho_\nu + \left(\Omega_{DE}^0 - 1 + \frac{3\lambda - 1}{2\xi - \eta} \right) \right]. \quad (46)$$

This is the background equation that EFTCAMB evolves, along with its time derivatives. For details about how the code treats ρ_ν see ref. [40]. Finally, one can use eq. (45), to substitute the “bare” cosmological constant with Ω_{DE}^0 , therefore in the following we use the latter as one of the Hořava parameters that we fit to data instead of $\bar{\Lambda}$.

We shall now specialize to some choices of the Hořava parameters, and derive the corresponding expansion history in order to visualize and discuss the effects of Hořava gravity, in particular for the H3 and H2 cases, on background cosmology. We choose the background values of the cosmological parameters to be $\Omega_b^0 h^2 = 0.0226$ for baryons, $\Omega_c^0 h^2 = 0.112$ for cold dark matter, $\Omega_\nu^0 h^2 = 0.00064$ for massive neutrinos and $H_0 = 70$ Km/s/Mpc, accordingly to the default CAMB parameters. Additionally, the parameters of the H3 case are chosen to be: $\lambda = 1.4$, $\xi = 0.9$, $\eta = 1.0$; while in the H2 case we set $\lambda = 1.4$ and $\eta = 1.0$. While the general trend of the modifications does not depend on the magnitude of the theory parameters, the above values are selected in order to enhance the effects and clearly display the changes with respect to the standard cosmological model, Λ CDM. Thus they have to be considered as illustrative examples because the values involved are significantly bigger than the observational bounds that we will derive in section 4. However, in both cases the choices of parameters respect the viability criteria discussed in section 2.4.

In panel (a) of figure 1 we can see the behaviour of the relative densities for matter (dark matter and baryons), radiation (photons and relativistic neutrinos), and effective dark energy, as defined in eqs. (44). One can notice that at early times the matter species display density values that are generally bigger than one, on the contrary the dark energy component assumes negative values. This can be explained as follows. The matter components are well behaved, with positively defined densities with a time evolution that is exactly the standard one (eq. (40)), as expected when working in Jordan frame. However, the expansion history changes as it is rescaled by a constant (eq. (46)), altering the time behaviour of the relative abundances. The effective dark energy balances this effect in order to respect the flatness condition. We argue that in this specific case the interpretation of the modification of gravity in terms of a fluid-like component is not well justified/posed, representing instead a genuine geometrical modification of the gravitational sector. This kind of behaviour for the effective dark energy component is commonly encountered in dynamical analysis studies of modified gravity models where the flatness condition is used as a constraint equation [65, 33]. From the left panel of figure 1, we can also notice that Hořava gravity does not affect the time of radiation-matter equality as the continuity equations for these species are not changed, as it is clearly highlighted by the yellow region in the figure.

Indeed Ω_m and Ω_r for all the models cross at the same value of the scale factor. On the other hand, the time of equality between matter and dark energy is slightly modified depending on the model parameters.

In panel (b) of figure 1, we can see the behaviour of $w_{\text{eff}} \equiv -1/3 - 2\dot{\mathcal{H}}/(3\mathcal{H}^2)$. We can clearly notice that the modifications induced by Hořava gravity result in a global rescaling of the effective equation of state, which, depending on the choice of the parameters, can lead to negative values of w_{eff} at late times. Finally, let us notice that, once the parameters of the theory are chosen to be compatible with the observational constraints, all these effects that we have discussed are quite mitigated and become hardly noticeable by eye in the plots. Values of the parameters consistent with the bounds that we derive in section 4 would induce a less negative DE density at earlier times. Furthermore, they would give an effective equation of state, w_{eff} , basically indistinguishable from the Λ CDM one.

3.2 Perturbations

In this section, we proceed to study the dynamics of cosmological perturbations. Once we have worked out the background equations of Hořava gravity (46), as well as the mapping of this theory into the EFT language (22), we have all the ingredients required by EFTCAMB to perform an accurate analysis of the perturbations. For technical details on the actual implementation, as well as the full set of perturbative equations that are evolved by EFTCAMB, we refer the reader to ref. [41].

As we will see, the behaviour of perturbations in Hořava gravity displays an interesting and rich phenomenology, allowing to investigate the theory and to constrain its parameters with the available data. In the following, we perform an in depth analysis of the dynamics of linear perturbations and the corresponding observables, specializing to a choice of parameters for the case H3 and one for the case H2, in order to visualize and quantify the modifications. In all cases, we set the values of the cosmological parameters to the one used in the previous section, which are the default CAMB parameters, while for the Hořava parameters we use: in the H3 case, $(\xi - 1) = -10^{-5}$, $(\lambda - 1) = 4 \times 10^{-4}$, $\eta = 10^{-3}$; in the H2 case, $(\lambda - 1) = 2 \times 10^{-3}$, $\eta = 5 \times 10^{-3}$. As it will be clear in the next section, these are noticeably bigger than the observational constraints that we will derive, but they facilitate the visualization of the effects on the observables. Let us stress that, while the direction and entity of the modifications that will be described in the remaining of this section are specific to the choice of parameters, we have found an analogous trend for several choices of parameters that we have sampled in the region allowed by the *viability priors*.

Let us now focus on the time and scale evolution of cosmological perturbations and the growth of structure. In order to discuss the deviations of Hořava gravity from Λ CDM, we study the behaviour of the $\mu(k, a)$ -function, which is defined in Newtonian gauge as [66]

$$k^2 \Psi \equiv -\mu(k, a) \frac{a^2}{2m_0^2} \rho_m \Delta_m, \quad (47)$$

where Δ_m is the comoving matter density contrast and Ψ is the scalar perturbation describing fluctuations in the time-time component of the metric. As it is clear from eq. (47), μ parametrizes deviations from GR in the Poisson equation. In the standard cosmological model, Λ CDM, this function is constant and $\mu = 1$. Let us notice that EFTCAMB does never evolve the above quantity (47), but it can easily output μ as a derived quantity. Moreover, we also analyse the behaviour of the quantity $\Phi + \Psi$, where Φ is the scalar perturbation of the space-space component of the metric in Newtonian gauge. This quantity is important as it allows to identify possible modifications in the lensing potential and in the low multipole of the cosmic microwave background (CMB) radiation through the Integrated Sachs-Wolfe (ISW) effect. Finally, we explore the fluctuations in the total matter distribution defined as $\delta_m \equiv \sum_m \rho_m \Delta_m / \sum_m \rho_m$.

In figure 2 we show the time and scale behaviour of these three quantities. In order to facilitate the visualization of the deviations from the Λ CDM behaviour, we show the logarithmic fractional comparison between these quantities in the two Hořava gravity cases considered and the Λ CDM model.

- *H3 case*: from the top right panel of figure 2 we can see that μ significantly deviates from one at small scales and all redshift with fractional differences that are above unity (100%). Significant deviations of the order of 10^{-2} (1%) can be also seen at large scales and high redshift. Close to the cosmological effective horizon we can notice that there is a region of scales and times where μ goes back to its GR value. At small scales, in the μ plot one can notice small features due to the fact that the π field oscillates while being coupled to the other species. From the top central panel of the same figure we can see that gravitational lensing is modified as well but with a rather simpler phenomenology. On large, super-horizon, scales deviations from the Λ CDM behaviour are not significant, staying well below 10^{-2} (1%) at all the times shown. On sub-horizon scales in turn the suppression of the lensing potential with respect to the Λ CDM case becomes relevant and just below the horizon it is above unity. A similar behaviour can be seen in the total matter density contrast. Noticeably the oscillations that we see in μ do not reflect on $\Phi + \Psi$ and δ_m , which look rather regular. The physical interpretation of this is that even if the additional scalar DoF is introducing fluctuations in the structure of the Poisson equation the field is not coupled strongly enough to introduce fast fluctuations in the matter and metric fields themselves.

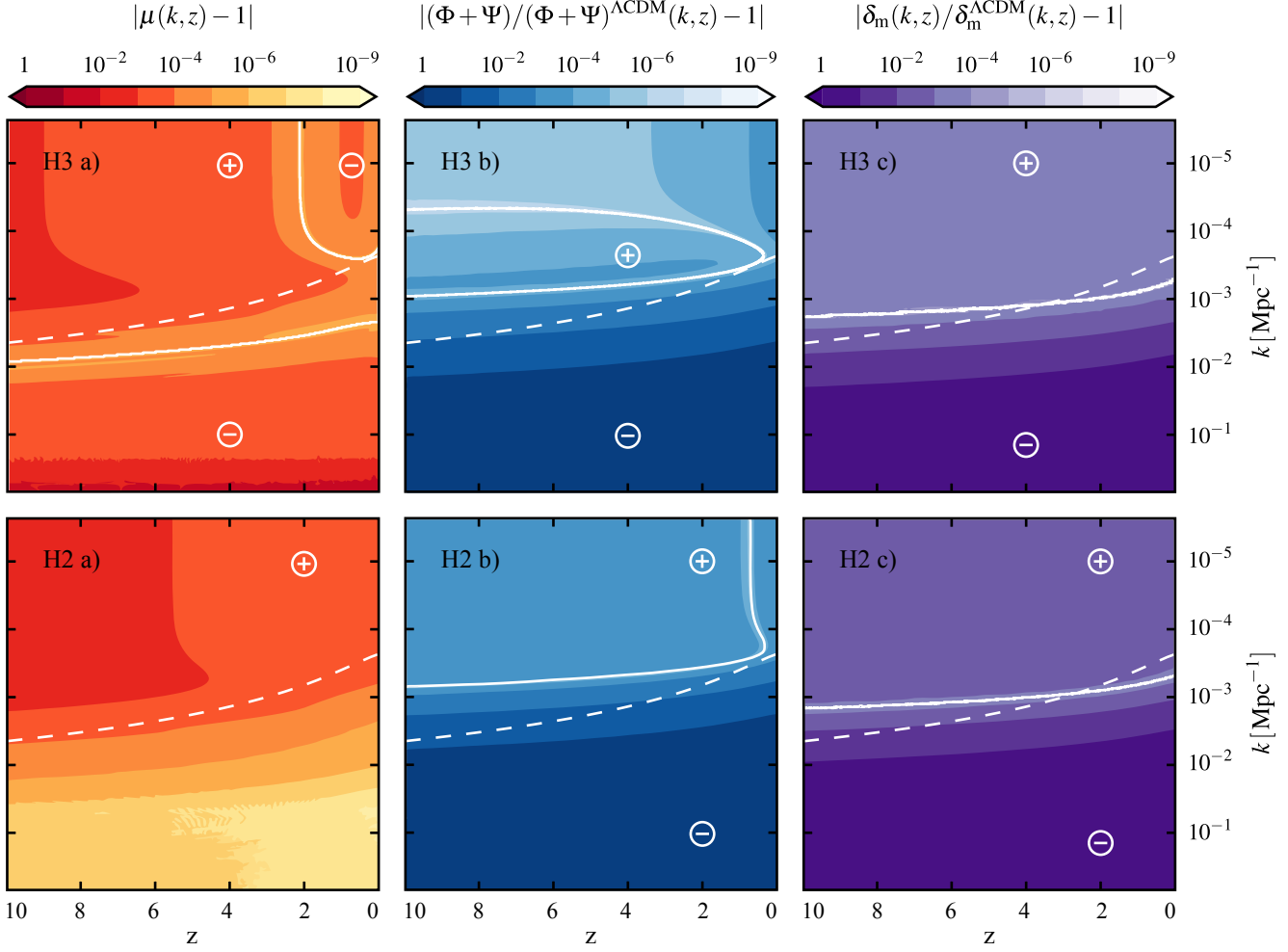


Figure 2: We show the relative comparison of the modification of the Poisson equation μ , the source of gravitational lensing $\Phi + \Psi$ (whose derivative sources the ISW effect on the CMB), and $\delta_m \equiv \sum_m \rho_m \Delta_m / \sum_m \rho_m$ with their Λ CDM values for the H3 (upper panel) and H2 (lower panel) models. In all panels, the dashed white line represents the physical horizon while the solid white line shows where the relative comparison changes sign. For this figure the standard cosmological parameters are chosen to be $\Omega_b^0 h^2 = 0.0226$, $\Omega_c^0 h^2 = 0.112$, $\Omega_\nu^0 h^2 = 0.00064$ and $H_0 = 70$ Km/s/Mpc. In the H3 case the additional parameters are $(\xi - 1) = -10^{-5}$, $(\lambda - 1) = 4 \times 10^{-4}$, $\eta = 10^{-3}$ while in the H2 case they are fixed to $(\lambda - 1) = 2 \times 10^{-3}$, $\eta = 5 \times 10^{-3}$. For a detailed explanation of this figure see section 3.2.

- *H2 case*: from the lower left panel of figure 2 we can notice that, in the H2 case, the behaviour of μ is rather different from the H3 case. In particular on small scales its value returns to the GR one. This is compatible with the extra constraint that we have imposed in this case (37), making the theory indistinguishable from GR on solar system scales. On large scales and high redshift, similarly to the H3 case, deviations from the Λ CDM behaviour are of the order 10^{-2} (1%). Panels H2 b) and H2 c) in figure 2 show that the lensing effects and the growth of matter perturbations do not follow the trend of μ . In fact as in the previous case on small, sub-horizon, scales the model displays significant deviations from the Λ CDM behaviour. As before dynamical oscillations of π are reflected on the behaviour of μ but do not show up in the other two quantities.

After considering the cosmological evolution of metric and matter perturbations we now turn to the study of the dynamics of the additional scalar DoF that propagates in Hořava gravity. In particular we study the quantity introduced in ref. [38] to quantify the deviations from quasi-staticity for the dynamical scalar DoF, π , i.e.

$$\xi_N = \frac{\dot{\pi}_N}{\mathcal{H}\pi_N}, \quad (48)$$

where with the index N we indicate that we are working with the π -field in Newtonian gauge. This quantity compares the evolutionary time-scale of the additional scalar DoF with the Hubble time scale, thus quantifying how many times

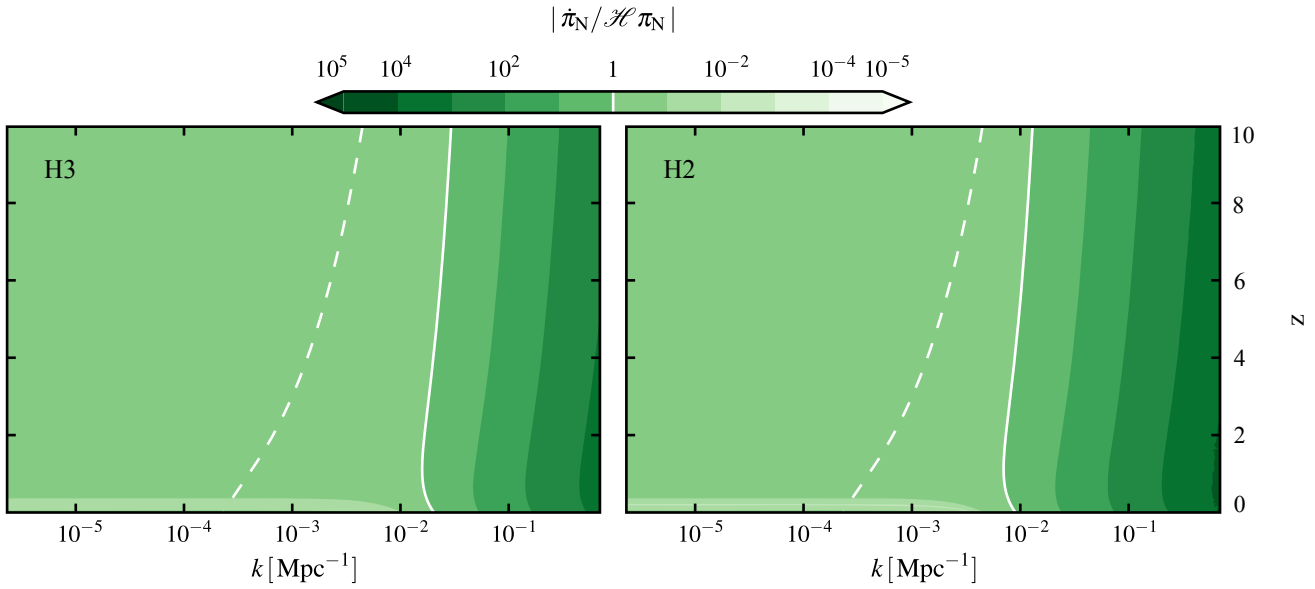


Figure 3: We show the quantity $\xi_N = \dot{\pi}_N / \mathcal{H} \pi_N$ that we introduce as an indicator of the goodness of the quasi-static approximation for the H3 (left panel) and H2 (right panel) cases. In both panels, the dashed white line represents the physical horizon, while the solid white line corresponds to values for which the evolutionary time scale of the π_N -field is the same as the Hubble time scale. For this figure the standard cosmological parameters are chosen to be $\Omega_b^0 h^2 = 0.0226$, $\Omega_c^0 h^2 = 0.112$, $\Omega_\nu^0 h^2 = 0.00064$ and $H_0 = 70 \text{ Km/s/Mpc}$. In the H3 case the Hořava gravity parameters are $(\xi - 1) = -10^{-5}$, $(\lambda - 1) = 4 \times 10^{-4}$, $\eta = 10^{-3}$ while in the H2 case they are fixed to $(\lambda - 1) = 2 \times 10^{-3}$, $\eta = 5 \times 10^{-3}$. For a detailed explanation of this figure see section 3.2.

the π -field changes significantly in a Hubble time. Small values of this quantity imply that the π field is slowly evolving and that time derivatives of the field can be neglected when compared to the value of the scalar field itself. On the contrary large values mean that the time derivative of the field is playing a major dynamical role, and hence QS would not be a safe assumption.

The time and scale behaviour of ξ_N can be seen, for the H3 and H2 cases, in figure 3. We can notice that, roughly for both cases, the π -field is slowly evolving on super-horizon scales in the redshift range that is shown. On the other hand, on small scales we can see that its dynamics becomes important as it starts to oscillate. In both panels of figure 3 the cross-over scale is shown as a solid white line, which separates the regime where the evolutionary time-scale of the π -field is smaller than the Hubble time scale from the region where the π -field is slowly evolving. This cross-over scale slightly depends on the model parameters, and for the ones chosen it is smaller than the cosmological effective horizon. At scales where ξ_N is below the cross-over scale, we can see that the time evolution of the scalar field is non-negligible and an eventual QS approximation would strongly break down.

Finally, we discuss how the modified dynamics of perturbations in Hořava gravity affects the observables that we later use to constrain this theory. In figure 4, we compare several power spectra for the H2 and H3 cases in comparison to the Λ CDM model. We identify the following effects on the observables:

- *Differences in the late time Integrated Sachs-Wolfe (ISW) effect.* For the two cases that we explore, we find an enhancement of the amplitude of the low- ℓ temperature power spectrum, as it can be seen from the top left panel of figure 4 which is related to an increase of the late-time ISW effect [67]. The latter is sourced by the time derivative of $\Phi + \Psi$ and, as we can see from figure 2, for the two Hořava gravity cases the time evolution of this quantity is modified. This change also affects the CMB temperature-lensing cross correlation (central left panel), as discussed below.
- *Differences in the gravitational lensing.* As we already discussed, in the specific cases that we explore, the gravitational lensing results to be suppressed, as we can see in the central panel of figure 2. This reflects on the CMB lensing power spectrum as shown in the central right panel of figure 4, where we can notice that fluctuations of this observable are suppressed for both H3 and H2 cases with respect to the Λ CDM model. This modification also has an effect on the high multipole of the lensed CMB temperature power spectrum as highlighted in the top-right panel of figure 4. At first glance we can see that, compared to the Λ CDM model, the profile of the high- ℓ peaks is much sharper in the H3 and H2 cases because of the lensing suppression. We can also notice that there is a slight asymmetry between peaks and troughs due to a combined effect of the lensing modification with

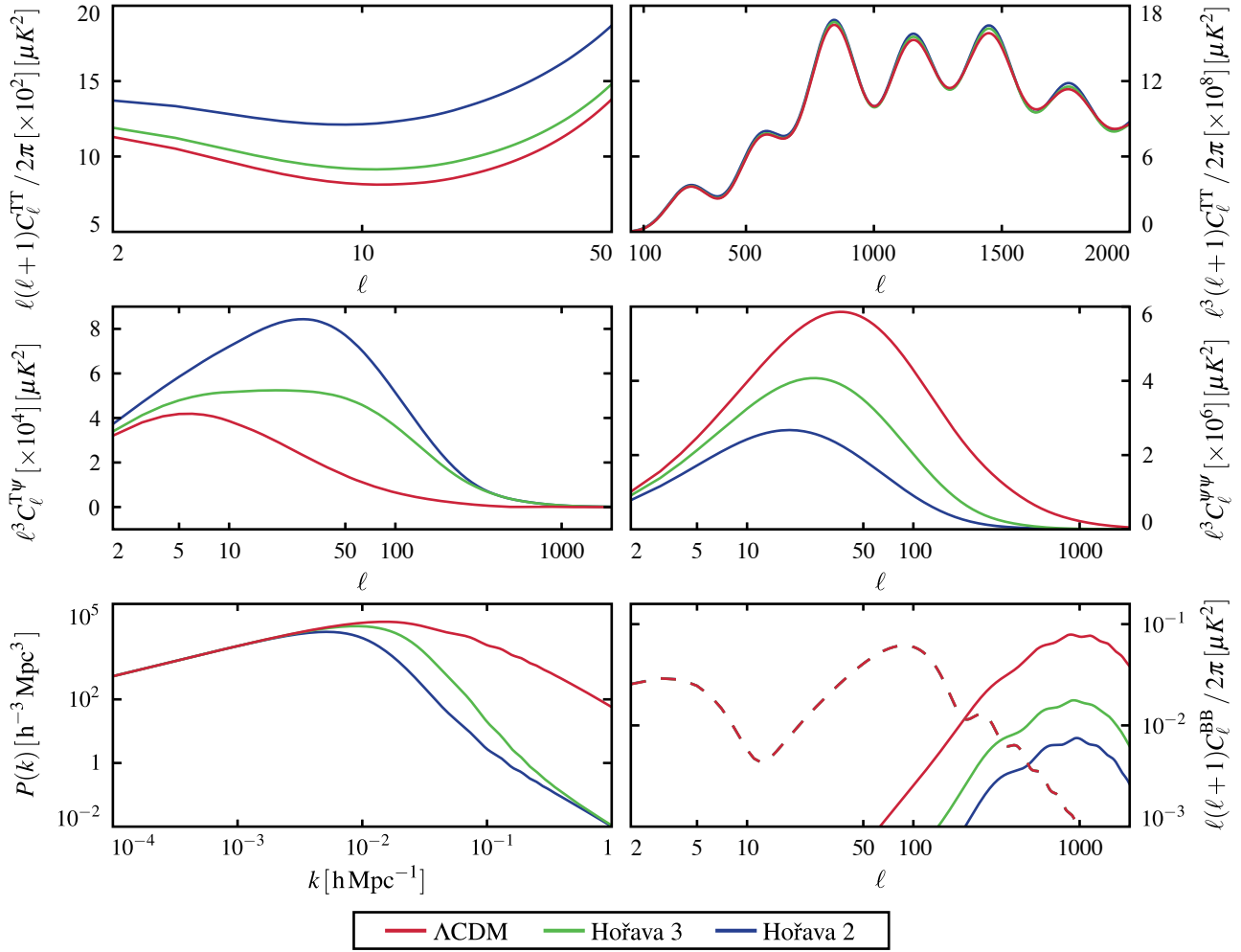


Figure 4: Power spectra of different cosmological observables in the Λ CDM, H2 and H3 cases. *Upper panel:* CMB temperature-temperature power spectrum at large (left) and small (right) angular scales. *Central panel:* lensing potential and CMB temperature cross correlation power spectrum (left), lensing potential auto correlation power spectrum (right). *Lower panel:* matter power spectrum (left) and B-mode polarization power spectrum (right). In this last panel the solid line correspond to the scalar induced B-mode signal while the dashed one shows the tensor induced component. For this figure the standard cosmological parameters are chosen to be $\Omega_b^0 h^2 = 0.0226$, $\Omega_c^0 h^2 = 0.112$, $\Omega_\nu^0 h^2 = 0.00064$ and $H_0 = 70$ Km/s/Mpc. The Hořava gravity parameters in H3 case are chosen to be: $(\xi - 1) = -10^{-5}$, $(\lambda - 1) = 4 \times 10^{-4}$, $\eta = 10^{-3}$; in the H2 case they are: $(\xi - 1) = 0$, $(\lambda - 1) = 2 \times 10^{-3}$, $\eta = 5 \times 10^{-3}$.

the modified Hubble rate discussed in section 3.1, thus leading to a small change in the angular scale of the CMB peaks. From the central left panel, we can see that the CMB temperature-lensing cross correlation spectrum is influenced by both the ISW and lensing modifications. In particular, this spectrum results to be enhanced as the cross correlation is dominated by the ISW effect. Finally, the suppression of the lensing potential also affects the component of the CMB B-mode power spectrum that is sourced by the lensing of the E-mode of polarization. This situation is highlighted in the lower right panel of figure 4. The solid lines representing this component of the B-mode spectrum are suppressed proportionally to the suppression in the lensing potential.

- *Differences in the growth of matter perturbations and the distribution of the large scale structure.* For the two cases under analysis (H3 and H2), we observe a suppression of the growth of structure in the total matter power spectrum as it is clearly depicted in the lower left panel of figure 4, and in agreement with our previous analysis of the time and scale dependence of the density contrast, see figure 2. As we already discussed, the modifications to the growth rate are scale dependent. Correspondingly, the matter power spectrum, for both H2 and H3, follows the Λ CDM one on large scales ($k \lesssim 10^{-3}$ h/Mpc) while for $k \gtrsim 10^{-3}$ h/Mpc it is greatly suppressed, particularly for the H2 case. At very small scales, both the H2 and H3 matter spectra tend to the same value, which is roughly four orders of magnitude smaller than the Λ CDM one.

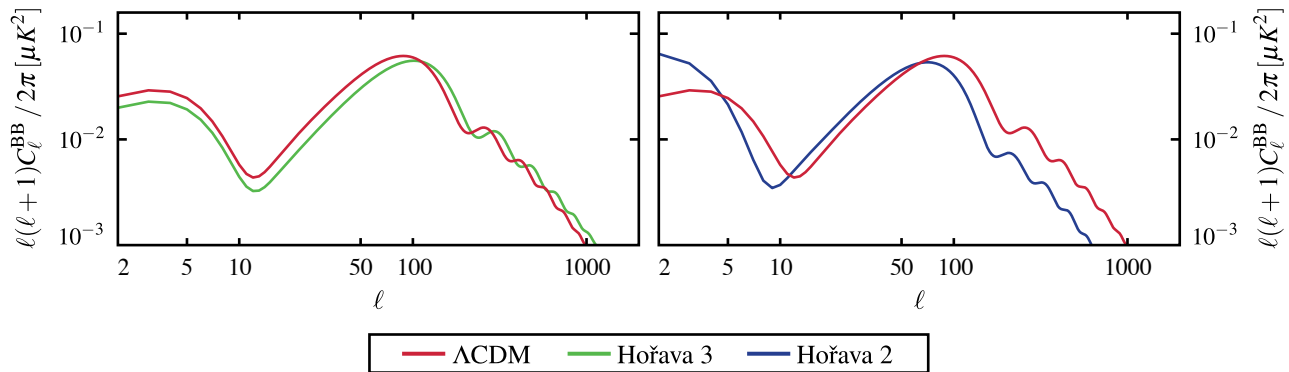


Figure 5: The tensor induced component of the B-mode CMB polarization power spectrum in the ΛCDM , H2 and H3 cases. For this figure the standard cosmological parameters are chosen to be $\Omega_b^0 h^2 = 0.0226$, $\Omega_c^0 h^2 = 0.112$, $\Omega_\nu^0 h^2 = 0.00064$, $r = 1$ and $H_0 = 70 \text{ Km/s/Mpc}$. The Hořava gravity parameters in H3 case are chosen to be: $(\xi - 1) = -0.3$, $(\lambda - 1) = 4 \times 10^{-4}$, $\eta = 10^{-3}$ in the H2 case they are: $(\lambda - 1) = 1$, $\eta = 0.6$.

- *Differences in the propagation of tensor modes.* As previously discussed in section 2.4, the tensor dynamical equation is modified in Hořava gravity. This change is usually reflected in the tensor induced component of the B-modes of CMB polarization [68, 69]. In particular, in the H3 case, the parameter ξ controls directly the propagation speed of gravitational waves, while the combination $2\xi - \eta$ is responsible for the strength of coupling between tensor modes and matter. Instead, in the H2 case the tensor speed of sound is controlled by η , while there is no effect on the coupling with matter. The choice of parameters we made for figure 4, displays a significant effect on the scalar component of the B-mode spectrum as shown in the lower right panel of figure 4 as solid lines, but the effect on the tensor component (dashed line) of the B-mode power spectrum for the same parameters is much smaller and not visible in the figure. In figure 5 we change the Hořava gravity parameters to better display the effect of the change in the tensor sector. Therefore only for this figure we choose the Hořava gravity parameters in H3 case to be $(\xi - 1) = -0.3$, $(\lambda - 1) = 4 \times 10^{-4}$, $\eta = 10^{-3}$ and in the H2 case they are $(\lambda - 1) = 1$, $\eta = 0.6$. As we can see from that figure, the leading effect is due to the modification of the speed of gravitational waves [69]. In the next section we will find that due to a combination of viability requirements and data constraints, for the H3 case $\xi < 1$, therefore the spectrum results to be shifted to the right with respect to the ΛCDM one, since tensor modes propagate sub-luminally. On the other hand, in the H2 case, tensor modes propagate super-luminally ($\eta > 0$) and the whole spectrum is shifted to the left. Finally, a modification of the coupling to matter leaves an observational imprint that is much smaller than the previous one as cosmological gravitational waves propagate almost in vacuum.

4 Cosmological constraints

In this section we derive and discuss the observational constraints on Hořava gravity coming from cosmological probes. After describing the data sets used, we focus on the H3 and H2 cases described at the end of section 2.4.

4.1 Data sets

In our analysis we use several geometrical and dynamical probes, combining them progressively.

The first data set employed, hereafter PLC, consists of the low- ℓ ($2 \leq \ell < 50$) CMB temperature-temperature power spectra from the *Planck* satellite [70, 71], considering the 9 frequency channels ranging from 30 \sim 353 GHz. In addition, we consider the 100, 143, and 217 GHz frequency channels for the high- ℓ modes ($50 \leq \ell \leq 2500$) of the CMB temperature spectrum. We also include the WMAP low- ℓ polarization spectra ($2 \leq \ell \leq 32$) [72] to break the degeneracy between the re-ionization optical depth and the amplitude of CMB temperature anisotropy.

The second data set considered, denoted as BG, is a combination of background measurements that helps to break the degeneracies between background parameters and the ones describing the behaviour of perturbations. We use data from HST [73] which measures the local Hubble constant from optical and infrared observations of more than 600 Cepheid variables. In addition, we consider the “Joint Light-curve Analysis” (JLA) Supernovae sample as analysed in ref. [74] which is constructed from the SNLS, SDSS and HST SNe data, together with several low redshift SNe. We also employ baryon acoustic oscillations measurements taken from: the SDSS Main Galaxy Sample at $z_{\text{eff}} = 0.15$ [75];

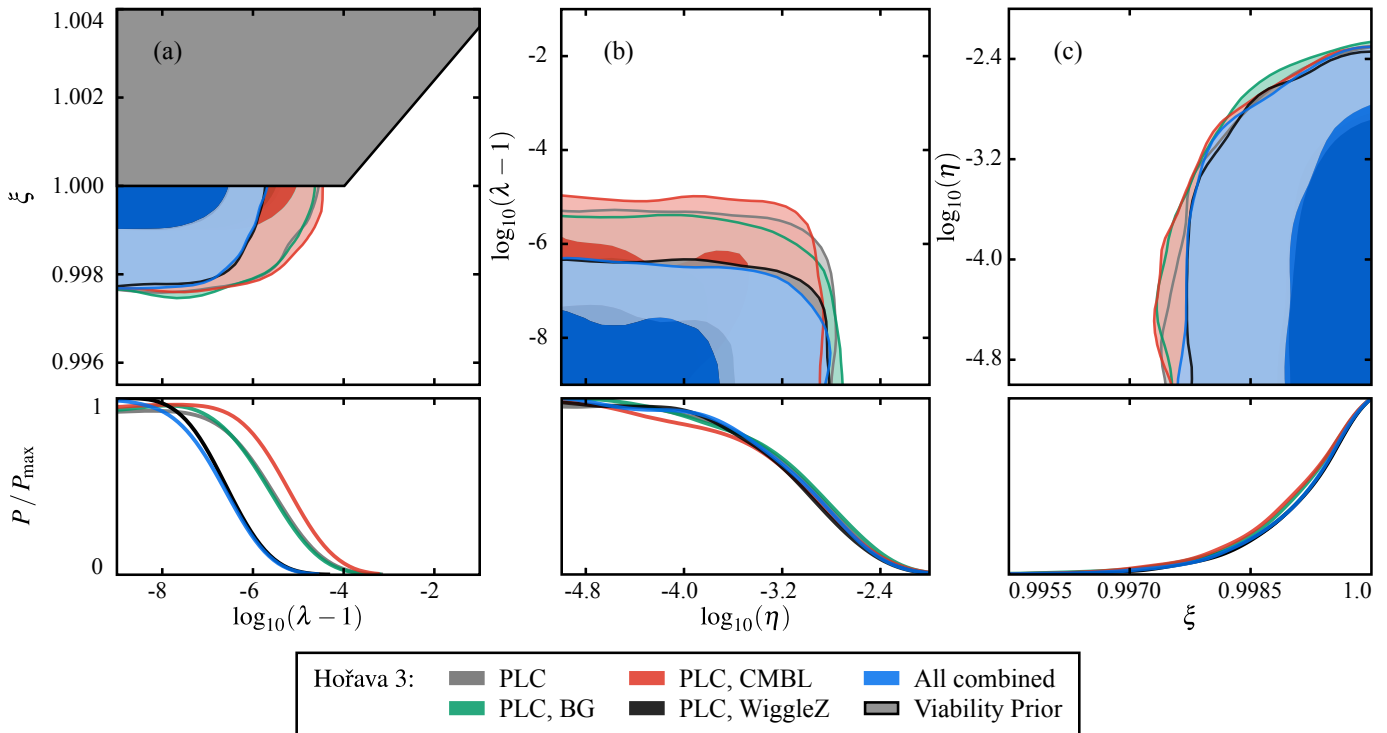


Figure 6: Results of our analysis of the H3 case. *Upper panel:* The marginalized joint likelihood for combinations of the parameters of low-energy Hořava gravity. The darker and lighter shades correspond respectively to the 68% C.L. and the 95% C.L.. *Lower panel:* The marginalized likelihood of the parameters of low-energy Hořava gravity. In both panels different colours correspond to different data set combinations as shown in legend. The dark grey shade corresponds to the marginalized region of parameter space excluded by *viability priors*.

the BOSS DR11 “LOWZ” sample at $z_{\text{eff}} = 0.32$ [76]; the BOSS DR11 CMASS at $z_{\text{eff}} = 0.57$ of [76]; and the 6dFGS survey at $z_{\text{eff}} = 0.106$ [77].

The third data set that we use, consists of the *Planck* 2013 full-sky lensing potential power spectrum obtained by using the 100, 143, and 217 GHz frequency bands employed by the *Planck* collaboration to detect the CMB lensing signal with a significance greater than 25σ [78]. We refer to this data set as the lensing one, hereafter CMBL.

Finally, we use the measurements of the galaxy power spectrum by the WiggleZ Dark Energy Survey [79] in order to exploit the constraining power of large-scale structure data. The WiggleZ data set consists of the galaxy power spectrum measured from spectroscopic redshifts of 170,352 blue emission line galaxies over a volume of 1 Gpc^3 [80, 81]. The covariance matrices are taken to be the ones given in ref. [81] and are computed using the method described in ref. [82]. It has been shown in refs. [81, 83] that linear theory predictions are a good fit to the data regardless of non-linear corrections up to a scale of $k \sim 0.2 \text{ h/Mpc}$. Since changes in the growth induced by modifications of gravity can slightly alter this scale, in this work, we use the WiggleZ galaxy power spectrum with a more conservative cut of $k_{\text{max}} = 0.1 \text{ h/Mpc}$. We marginalize over a scale independent linear galaxy bias for each of the four redshift bins, as in ref. [81].

4.2 H3 case: results

The first case we compare to cosmological observations is the low-energy limit of Hořava gravity, H3, for which the parameters of the theory are $\{\xi, \lambda, \eta\}$.

We sample λ and ξ shifting them by one so that the GR limit of the new parameters, i.e. $\lambda - 1$ and $\xi - 1$, corresponds to a zero value. In addition, we use a logarithmic sampler for the parameters η and $\lambda - 1$ as they are constrained to be positive by physical viability, as discussed at length in section 2.4. Instead, ξ is allowed to change sign, hence we sample $\xi - 1$ linearly.

When combining the *viability priors* discussed in section 2.4, with cosmological data, we notice that the requirement of physical viability has a strong effect on the posterior distribution of the parameter ξ . This is shown in panel (a) of figure 6. Even though ξ is not constrained to be above or below 1 a priori, the magnitude of λ , draws the posterior of the model into a region where only values of $\xi \leq 1$ are viable. Let us notice that there is a very small viable region

Parameters	H3 case				
	PLC	PLC+BG	PLC+CMBL	PLC+WiggleZ	all combined
$\xi - 1^{(*)}$	> -0.0039	> -0.0042	> -0.0038	> -0.0038	> -0.0038
$\log_{10}(\lambda - 1)$	< -5.1	< -5.2	< -5.0	< -6.2	< -6.2
$\log_{10} \eta$	< -2.4	< -2.4	< -2.4	< -2.4	< -2.4
Ω_{DE}^0	$0.68^{+0.04}_{-0.05}$	$0.69^{+0.02}_{-0.02}$	$0.68^{+0.03}_{-0.06}$	$0.66^{+0.04}_{-0.05}$	$0.69^{+0.02}_{-0.02}$
α_1	< 0.033	< 0.035	< 0.033	< 0.032	< 0.032
$\log_{10} \alpha_2$	< 10.9	< 10.9	< 10.8	< 10.8	< 10.8
$G_{\text{cosmo}}/G_N - 1$	< 0.0041	< 0.0043	< 0.0042	< 0.0039	< 0.0040

Table 1: The 99.7% C.L. marginalized posterior bounds on the H3 case parameters and relevant derived parameters. (*) Let us notice that the combination of stability conditions and observational constraints set also an upper bound on this parameter, i.e. $\xi - 1 < 0$.

in the parameter space above one ($1 < \xi \lesssim 10^{-6}$), which due to the scale adopted in the plot cannot be seen by eye; however, since this is significantly smaller than the region below $\xi = 1$, it is not picked up when sampling linearly the parameter ξ . As we can see from the other two panels of figure 6, the *viability priors* do not have a strong impact on λ and η in the region where the posterior of the model is peaked.

From the top panels of figure 6, we can notice that the different parameters specifying Hořava gravity do not have sizable degeneracies between them over all the range explored (which spans several orders of magnitude). From the lower panel of the same figure we can notice that different data sets contribute differently to the bounds on λ , while the constraints on the other two parameters are dominated by PLC and hence do not change much when other data sets are added. In particular the WiggleZ data set drives the most stringent constraints on λ and the total data sets combination is dominated by it, driving the posterior of λ to very small values. The PLC and the PLC+BG data sets, on the other hand, result in similar bounds on λ , mostly because, as commented in section 3, the changes induced by Hořava gravity on cosmological perturbations are larger than the ones induced on the background. Noticeably, the combination of PLC and CMBL results in slightly weaker constraints. This is mostly due to the fact that Hořava gravity suppresses the growth of structure and hence the lensing of the CMB (see figure 4). The *Planck* 2013 and the *Planck* 2015 data, in turn, favour a smaller amplitude of the CMB lensing power spectrum as reconstructed from the CMB trispectrum [71, 84, 85] and hence its addition to the data set combination drives the posterior to slightly higher values of λ in order to balance this effect. These results are confirmed by the marginalized bounds on the H3 parameters reported in table 1. The 99.7% C.L. bounds on the ξ and η parameters weakly depend on the data set used while the addition of large scale structure data strongly impacts the bounds on λ . As discussed in section 3.1, the “bare” cosmological constant $\bar{\Lambda}$ has been replaced in this analysis by Ω_{DE}^0 , and the latter has been included in table 1. The most relevant result that can be drawn from table 1 is that low-energy Hořava modifications of gravity are severely constrained, with the corresponding parameters bounded to be orders of magnitude below unity. In particular, we find that cosmological data have a strong constraining power on λ . Here we summarize the bounds, at 99.7% C.L, that we get from the combination of all data sets:

$$\begin{aligned}
\xi - 1 &> -0.0038, \\
\log_{10}(\lambda - 1) &< -6.2, \\
\log_{10}(\eta) &< -2.4, \\
\Omega_{DE}^0 &= 0.69^{+0.02}_{-0.02}.
\end{aligned} \tag{49}$$

Let us notice that the *viability priors* give also an upper bound on ξ , i.e. $\xi < 1$. All the standard derived cosmological parameters for this case are compatible to the Λ CDM model as shown in appendix B.

In table 1 we report also the marginal bounds on the PPN parameters $\{\alpha_1, \alpha_2\}$ and $G_{\text{cosmo}}/G_N - 1$. From the first two, we can notice the extreme complementarity of cosmological and solar system experiments in constraining Hořava gravity. Cosmological observations constrain α_1 at percent level while PPN bounds on this parameter are two orders of magnitude stronger. However, cosmological observations are sensitive to both ξ and η , while solar system probes constrain just a degenerate combination of the two. On the other hand the cosmological bounds on the α_2 parameter are worst than the PPN ones by several orders of magnitude. That is due to the fact that in the limit in which λ is constrained to be much smaller than the other parameters by cosmological data, the α_2 parameter goes to infinity as it is clear from its definition (35). Then, if we compare the cosmological constraint on λ with the one that is derived from α_2 in eq. (36), we see that our bounds are two orders of magnitude stronger than solar system constraints. Finally, we

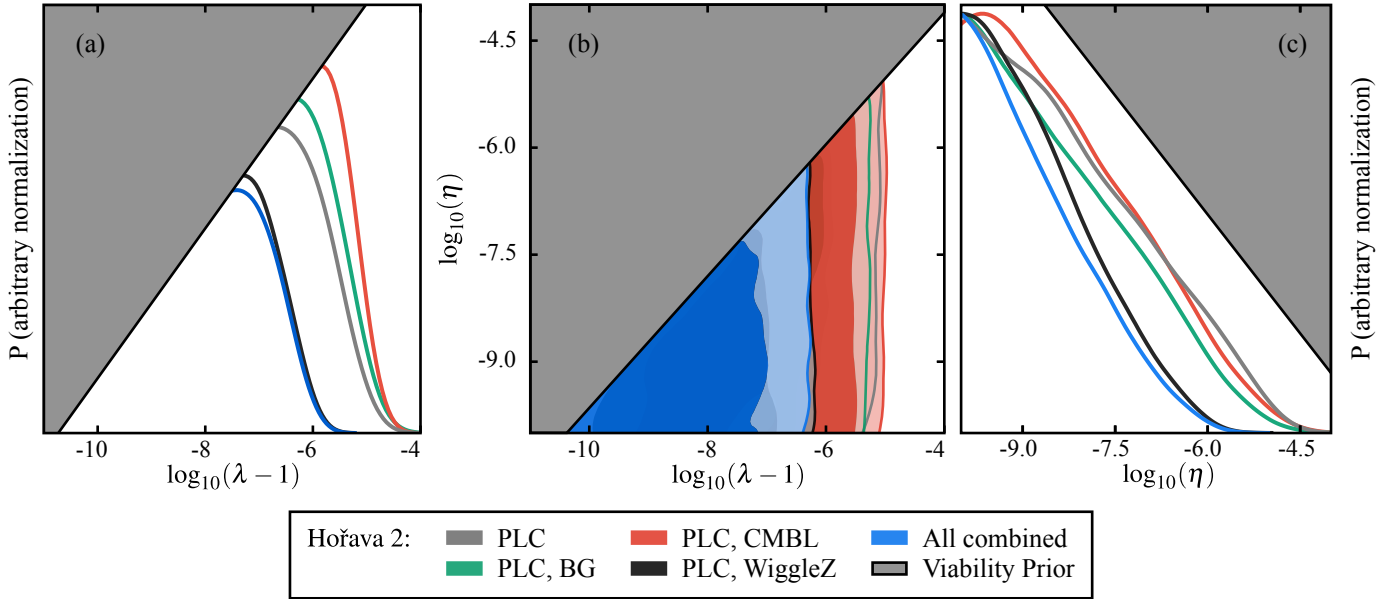


Figure 7: Results of our analysis of the H2 case. *Panel (a)*: The marginalized likelihood of $\log_{10}(\lambda - 1)$; *Panel (b)*: The marginalized joint likelihood of $\log_{10}(\lambda - 1)$ and $\log_{10}\eta$. The darker and lighter shades correspond respectively to the 68% C.L. and the 95% C.L.. The theoretical viability condition is roughly $(\lambda - 1) > \mathcal{O}(2\eta/9)$; *Panel (c)*: The marginalized likelihood of $\log_{10}\eta$. In all panels different colours correspond to different data set combinations as shown in legend. The dark grey shade corresponds to the marginalized region of parameter space excluded by *viability priors*. The arbitrary normalization of the posterior is chosen to better display the effect of the *viability priors*.

can see that the bound on $G_{\text{cosmo}}/G_N - 1 < 0.0040$ (99.7% C.L., all combined) is improved by two orders of magnitude with respect to previous results [11].

4.3 H2 case: results

The second case we consider, is a sub-case of the previous one obtained by restricting to the plane of the parameter space corresponding to $\eta = 2\xi - 2$. For this choice, the solar system constraints are automatically evaded as shown by studies of the PPN limit of Hořava gravity (see section 2.4). We refer to this as the H2 case. The free parameters of the theory are now $\{\eta, \lambda\}$ and, as discussed in the previous section, we sample the parameter space of the logarithm of η and $\lambda - 1$ since both these quantities are constrained by the *viability priors* to be positive. Unlike for the H3 case, where the *viability priors* had a strong influence only on the parameter ξ , in the H2 case they have a strong influence on the marginalized posterior for both η and λ , as one can see in figure 7. In particular one can notice in panel (b) of figure 7 that the viable region is a triangle corresponding roughly to the condition $(\lambda - 1) > \mathcal{O}(2\eta/9)$. This triangle shape of the marginalized joint posterior of the model parameters has a strong influence on the marginalized 1D posterior of the two parameters. In particular, as we can see in panel (a) of figure 7, the low tail of λ is cut by the *viability priors* and, in panel (c), the posterior of η becomes markedly non-gaussian. Apart from the degeneracy induced by this prior cut, no other degeneracy between the Hořava gravity parameters is present.

In panel (a) of figure 7, we can see that different data sets contribute differently to the cosmological bounds. In particular the WiggleZ data set is pushing the posterior of λ to smaller values dominating the bounds coming from the total data set combination. The PLC and PLC+BG data sets instead give comparable bounds; the constraints become slightly weaker when considering CMB lensing for the same reasons explained in the previous section. Because of the degeneracy induced by the *viability priors*, the bounds on η are pushed to much smaller values with respect to the H3 case. These considerations are further confirmed by the marginalized confidence bounds on the parameters as reported in table 2. In this table we can notice that the 99.7% C.L. confidence bounds on λ are comparable to the previous ones while the bounds on η are considerably stronger. Indeed the bounds for all combination of data sets for the H2 case are:

$$\begin{aligned}
 \log_{10}(\lambda - 1) &< -5.9, \\
 \log_{10}(\eta) &< -6.1, \\
 \Omega_{DE}^0 &= 0.69^{+0.02}_{-0.02}.
 \end{aligned} \tag{50}$$

	H2 case				
Parameters	PLC	PLC+BG	PLC+CMBL	PLC+WiggleZ	all combined
$\log_{10}(\lambda - 1)$	< -4.8	< -4.9	< -4.5	< -5.9	< -5.9
$\log_{10} \eta$	< -4.8	< -5.1	< -4.9	< -6.0	< -6.1
Ω_{DE}^0	$0.68^{+0.04}_{-0.05}$	$0.69^{+0.02}_{-0.02}$	$0.68^{+0.03}_{-0.06}$	$0.66^{+0.04}_{-0.05}$	$0.69^{+0.02}_{-0.02}$
$G_{\text{cosmo}}/G_N - 1$	$< 2.1 \times 10^{-5}$	$< 1.7 \times 10^{-5}$	$< 1.9 \times 10^{-5}$	$< 1.7 \times 10^{-6}$	$< 1.5 \times 10^{-6}$

Table 2: The 99.7% C.L. marginalized posterior bounds on the H2 case parameters and $G_{\text{cosmo}}/G_N - 1$.

As in the previous case Ω_{DE}^0 and all the standard derived cosmological parameters are the same as in Λ CDM and H3 case. We report them in appendix B.

Noticeably in the H2 case, the bounds on $G_{\text{cosmo}}/G_N - 1$ ($< 1.5 \cdot 10^{-6}$, 99.7% C.L., all combined) are more stringent than in the H3 case. In particular this bound is several orders of magnitude stronger than the BBN bound.

5 Conclusion

In this paper we have performed a thorough investigation of the cosmology of Hořava gravity, which is a Lorentz violating theory proposed as a candidate for quantum gravity [16, 17]. The emergence of Lorentz violations at all scales, makes the theory power-counting renormalizable at very high energies ($\sim 10^{19}$ GeV/ c^2). However, since at low energies we do not experience LV effects, we expect large scales tests to place important constraints on the theory. In particular, we have analysed Hořava gravity at cosmological scales, to see whether there is any room for LV at these energies. As we will summarize in details in the following, we have found that cosmological data severely constrain Hořava gravity.

We have performed our analysis within the EFT framework for dark energy and modified gravity [28, 29], which we have reviewed in section 2.2. We have focused on the dynamics of the background and linear perturbations, and considered the power-counting renormalizable action for Hořava gravity which includes all the *quadratic* operators with up to sixth spatial derivatives [46]. For this action, we have worked out a complete mapping into the EFT language, in section 2.3, finding that its low-energy part is completely mapped in the most commonly used EFT action (7). While the high-energy part requires the inclusion of additional operators, that we have identified in appendix A. After working out the full mapping, when exploring the cosmology and corresponding observational bounds, in sections 3 and 4, we have restricted to the low-energy part of the action which is sufficient for a first exploration of the large scale phenomenology of the theory.

For our analysis we have made use of the powerful EFTCAMB/EFTCosmoMC package [38, 39, 41]. While this package was made publicly available by some of the authors at <http://wwwhome.lorentz.leidenuniv.nl/~hu/codes/>, for our analysis we have used an updated version which fully implements Hořava gravity. By the latter we mean that, for the first time, we have implemented in EFTCAMB a *full mapping* case, solving the Hořava equations for the background, instead of using a *designer* approach to the expansion history. We have included a detailed discussion of this procedure in section 3.1. After solving the background and before proceeding to the evolution of the perturbations, EFTCAMB runs a check on the viability of the selected theory, enforcing some stability requirements such as the absence of ghosts and gradient instabilities. The latter conditions become *viability priors* when using EFTCosmoMC to constrain the parameters of the theory by means of cosmological data. Finally, we have proceeded to evolve linear scalar perturbations with the general EFT equations [41], specializing their coefficients to the corresponding expressions in the Hořava case through the mapping worked out in section 2.3.

Let us notice that besides the physical stability requirements, Lorentz violations can also be constrained via BBN and solar system tests, as discussed at length in section 2.4. In our analysis we have not imposed the BBN experimental bounds a priori, rather we have compared them to our finding for cosmological constraints. Nevertheless, we have investigated two cases: a first one, H3, where the low-energy Hořava gravity parameters $\{\lambda, \xi, \eta\}$ were allowed to vary freely; the second case, H2, where we enforced a relationship between the parameters that allows the theory to evade PPN constraints, reducing the number of free parameters to two, $\{\lambda, \eta\}$.

In section 3, we have studied in details the cosmology of Hořava gravity. At background level, we have found a constant rescaling of the Hubble rate which reflects in the behaviour of the density parameters. Indeed, as shown in figure 1, the fractional matter density exceeds unity at all times and the fractional density of the effective dark energy (44) correspondingly becomes negative, so that the flatness condition is satisfied at all times. This behaviour signals that the modifications of gravity in this theory should be considered as a purely geometrical effect, rather than be interpreted in terms of a dark fluid. At the level of linear perturbations we have identified modifications in the

ISW effect, the gravitational lensing, the rate of growth of structure and the B-modes spectrum, which translated into stringent bounds on the Hořava parameters when we fit them to cosmological data. In order to facilitate a in depth visualization of characteristic features of Hořava gravity at the level of perturbations, we have specialized to two choices of parameters, one for the H3 case and one for the H2 case, and have performed a thorough analysis of the dynamics of perturbations and the corresponding cosmological observables. In both cases, we have found a general suppression of the growth of matter perturbations and the lensing potential. The first modifies the shape of the matter power spectrum, which we have found to be strongly suppressed for $k > 10^{-3}$ h/Mpc; the second one impacts the CMB temperature power spectrum at small angular scale and the CMB lensing power spectrum. In particular in the latter case the effect is of a general suppression of power in the lensing potential auto spectrum. A modification of the lensing potential also alters the scalar perturbation induced component of the B-mode power spectrum, leading to a decrease in that signal. On the other hand, we found an enhancement of the CMB temperature power spectrum at large angular scales and its cross-correlation with the lensing potential. This effect can be traced back to an enhancement of the ISW effect at late times. Finally, the tensor power spectrum is also modified as the speed of sound of the tensor modes depends on the parameters of the theory. In particular the tensor BB-power spectrum is shifted on the right with respect to the Λ CDM one for the H3 case as the tensor propagation is sub-luminal and on the left for H2 because the propagation is super-luminal. Noticeably, we have determined that in general the quasi-static approximation is not safe to describe the evolution of sub-horizon perturbations in Hořava gravity. Let us stress that while the direction and entity of these modifications is dependent on the specific choice of parameters, we have found a general suppression of the growth rate and lensing potential, and an enhancement of the ISW effect for several choices of parameters that we have sampled in the region allowed by the *viability priors*.

In section 4, we have moved on to perform a global fit of the two cases of low-energy Hořava gravity, H3 and H2, to progressive combinations of cosmological data sets: the CMB temperature-temperature and lensing power spectra by *Planck* 2013, WMAP low- ℓ polarization spectra, the WiggleZ galaxy power spectrum, the local Hubble measurements and Supernovae data from SNLS, SDSS and HST and the BAO measurements from BOSS, SDSS and 6dFGS.

In the case of H3, we have set upper bounds on $\{\lambda, \eta\}$ and a lower bound on ξ , while for $\Omega_{DE}^{(0)}$ (which through eq. (45) replaces $\bar{\Lambda}$) we found a mean value and errors that are very close to the ones of the Λ CDM model. Specifically we obtained $\xi - 1 > -0.0038$, $\log_{10}(\lambda - 1) < -6.2$, $\log_{10}(\eta) < -2.4$ and $\Omega_{DE}^0 = 0.69_{-0.02}^{+0.02}$ at 99.7% C.L. for the combination of all the data sets considered. For all the other data set combinations see table 1. Let us notice that in this case ξ has also an upper bound, i.e. $\xi < 1$ due to the combination of stability and cosmological constraints. As a general result we have found that the values of the Hořava gravity parameters are severely constrained to be close to their values in the GR limit, while the cosmological parameters have mean values and bounds very close to those of the Λ CDM model. For both cases we reported the constraints on the standard cosmological parameters in table 2. Moreover, for the H3 case we get an improved bound on $G_{cosmo}/G_N - 1 < 0.0040$ (99.7% C.L., for the combination of all data sets) which outruns the BBN one. On the other hand PPN experiments are two orders of magnitude stronger in constraining the α_1 parameter that we find to be $\alpha_1 < 0.032$ (99.7% C.L., for the combination of all data sets), while our cosmological bound on λ is two orders of magnitude stronger than the one derived from solar system tests.

For the H2 case, we were able to set upper bounds on $\log_{10}(\lambda - 1) < -5.9$ and $\log_{10}(\eta) < -6.1$ and constraints on $\Omega_{DE}^0 = 0.69_{-0.02}^{+0.02}$ at 99.7% C.L. with all data sets. Noticeably for this model we get a quite stringent bound on $G_{cosmo}/G_N - 1 < 1.5 \cdot 10^{-6}$ at 99.7% C.L. by combining all the considered data sets.

We plan to release the full mapping of the low-energy limit of Hořava gravity in the forthcoming update of the public version of EFTCAMB/EFTCosmoMC. As part of future work, it would be certainly of interest to explore the phenomenology associated to the high-energy part of the Hořava gravity action to see whether additional operators can affect significantly linear perturbations. Future analysis could also include the study of LV in the dark matter sector.

Acknowledgements

We are grateful to Carlo Baccigalupi and Enrico Barausse for useful discussions and comments on the manuscript. The research of NF and DV has received funding from the European Research Council under the European Community's Seventh Framework Programme (FP7/2007-2013, Grant Agreement No. 307934). MR acknowledges partial support from the INFN-INDARK initiative. BH is supported by the Dutch Foundation for Fundamental Research on Matter (FOM). AS acknowledges support from The Netherlands Organization for Scientific Research (NWO/OCW), and also from the D-ITP consortium, a program of the Netherlands Organisation for Scientific Research (NWO) that is funded by the Dutch Ministry of Education, Culture and Science (OCW).

A The L_4 and L_6 Lagrangians

The L_4 and L_6 Lagrangians contain, respectively, all the operators up to fourth and sixth order spatial derivatives, which are compatible with the symmetry of Hořava gravity and guarantee its power-counting renormalizability. The number of those operators is very large, but given that we are interested in an effective field theory description of linear scalar perturbations, only the ones which are second order in perturbations have to be considered in the action. The latter have been identified in ref. [46] and they are given by suitably contracting the three-dimensional Ricci tensor and scalar, the acceleration a_i , and their spatial derivatives. In detail, the HE part of action (3) can be written as

$$\begin{aligned} \mathcal{S}_{H,HE} = & \frac{1}{16\pi G_H} \int d^4x \sqrt{-g} (g_1 \mathcal{R}^2 + g_2 \mathcal{R}_{ij} \mathcal{R}^{ij} + g_3 \mathcal{R} \nabla_i a^i + g_4 a_i \nabla^2 a^i \\ & + g_5 \mathcal{R} \nabla^2 \mathcal{R} + g_6 \nabla_i \mathcal{R}_{jk} \nabla^i \mathcal{R}^{jk} + g_7 a_i \nabla^4 a^i + g_8 \nabla^2 \mathcal{R} \nabla_i a^i) \end{aligned} \quad (51)$$

where $\nabla^2 = \nabla^i \nabla_i$ and $\nabla^4 = \nabla^i \nabla_i \nabla^j \nabla_j$, and the coefficients g_i are running coupling constants of suitable dimensions. The first and second lines contain respectively the contributions from L_4 and L_6 .

We expand now the above action up to second order in perturbations by considering that on a flat FRLW background the components of \mathcal{R} and \mathcal{R}_{ij} identically vanish. Then we map it into the language at the basis of the EFT formalism discussed in section 2.2 by using the relation (19) for a_i . With these recipes, it is straightforward to show that the operators in action (51) up to second order can be written as

$$g_1 \frac{m_0^2}{(2\xi - \eta)} \mathcal{R}^2 = g_1 \frac{m_0^2}{(2\xi - \eta)} (\delta\mathcal{R})^2, \quad (52a)$$

$$g_2 \frac{m_0^2}{(2\xi - \eta)} \mathcal{R}_{ij} \mathcal{R}^{ij} = g_2 \frac{m_0^2}{(2\xi - \eta)} \delta\mathcal{R}_{ij} \delta\mathcal{R}^{ij}, \quad (52b)$$

$$g_3 \frac{m_0^2}{(2\xi - \eta)} \mathcal{R} \nabla_i a^i = g_3 \frac{m_0^2}{2(2\xi - \eta)} \delta\mathcal{R} \nabla^2 (a^2 \delta g^{00}), \quad (52c)$$

$$g_4 \frac{m_0^2}{(2\xi - \eta)} a_i \nabla^2 a^i = g_4 \frac{m_0^2}{4(2\xi - \eta)} \partial_i (a^2 g^{00}) \nabla^2 \partial^i (a^2 g^{00}), \quad (52d)$$

$$g_5 \frac{m_0^2}{(2\xi - \eta)} \mathcal{R} \nabla^2 \mathcal{R} = g_5 \frac{m_0^2}{(2\xi - \eta)} \delta\mathcal{R} \nabla^2 \delta\mathcal{R}, \quad (52e)$$

$$g_6 \frac{m_0^2}{(2\xi - \eta)} \nabla_i \mathcal{R}_{jk} \nabla^i \mathcal{R}^{jk} = g_6 \frac{m_0^2}{(2\xi - \eta)} \nabla_i \delta\mathcal{R}_{jk} \nabla^i \delta\mathcal{R}^{jk}, \quad (52f)$$

$$g_7 \frac{m_0^2}{(2\xi - \eta)} a_i \nabla^4 a^i = g_7 \frac{m_0^2}{4(2\xi - \eta)} \partial_i (a^2 \delta g^{00}) \nabla^4 (\partial^i (a^2 \delta g^{00})), \quad (52g)$$

$$g_8 \frac{m_0^2}{(2\xi - \eta)} \nabla^2 \mathcal{R} \nabla_i a^i = g_8 \frac{m_0^2}{2(2\xi - \eta)} \nabla^2 \delta\mathcal{R} \nabla^2 (a^2 \delta g^{00}). \quad (52h)$$

We notice immediately that the EFT action (7) is incomplete if one wants to treat the full version of Hořava gravity (which includes the operators in action (51)), then we need to add to it all the operators in eqs. (52). This suggests to extend the EFT action discussed in section 2.2 to a more general one by adding the following part:

$$\begin{aligned} \mathcal{S}_{EFT,2} = & \int d^4x \sqrt{-g} [\lambda_1(\tau) (\delta\mathcal{R})^2 + \lambda_2(\tau) \delta\mathcal{R}_{ij} \delta\mathcal{R}^{ij} + \lambda_3(\tau) \delta\mathcal{R} \nabla^2 (a^2 \delta g^{00}) + \lambda_4(\tau) \partial_i (a^2 g^{00}) \nabla^2 \partial^i (a^2 g^{00}) \\ & + \lambda_5(\tau) \delta\mathcal{R} \nabla^2 \delta\mathcal{R} + \lambda_6(\tau) \nabla_i \delta\mathcal{R}_{jk} \nabla^i \delta\mathcal{R}^{jk} + \lambda_7(\tau) \partial_i (a^2 \delta g^{00}) \nabla^4 (\partial^i (a^2 \delta g^{00})) + \lambda_8(\tau) \nabla^2 \delta\mathcal{R} \nabla^2 (a^2 \delta g^{00})]. \end{aligned} \quad (53)$$

In the Hořava gravity case the EFT functions λ_i 's reduce to the constant coefficients in eqs. (52), e.g. $\lambda_1 = g_1 m_0^2 / (2\xi - \eta)$.

Notice that the first two operators in the action (53) have already been considered in ref. [30], while the remaining operators have been considered in ref. [45]. However, in the latter work an explicit EFT action (in the form of the action (53)) has not been emphasized as well as an explicit mapping between these operators and a specific theory has not been worked out. In this respect our finding corresponds to new results. Finally, let us mention that although we wrote the operators in eqs. (52) in terms of 3D quantities, following the 3+1 formalism employed in Hořava gravity, one can always express them by means of 4D quantities by using the Gauss-Codazzi relation [57].

It would be of interest to implement the contributions of these new operators in the equations for the perturbations evolved in EFTCAMB, in order to investigate their cosmological effects. We expect that their contribution becomes more important as the cosmological scale becomes smaller. This is part of ongoing work [86].

B Cosmological Parameters

In this appendix we report the 99.7% C.L. constraints on the derived cosmological parameters: $\Omega_b^0 h^2$ the present day density parameter of baryons; $\Omega_c^0 h^2$ the present day value of the cold dark matter density parameter; $100\theta_{MC}$ which measures the sound horizon at last scattering; τ is the Thomson scattering optical depth due to reionization; n_s the power law index of the scalar spectrum; $\ln(10^{10} A_s)$ the log power of the primordial curvature perturbation, H_0 (km/s/Mpc) the present time value of the Hubble rate, and Ω_m^0 the dark matter density parameter today. We found that the constraints on these parameters for H3 and H2 are the same as in Λ CDM as reported in the following table. The reason for this is that Hořava gravity parameters are constrained to be very close to the GR limit so that the cosmological parameters fall back to their Λ CDM values.

Bounds on cosmological parameters for Λ CDM, H3 and H2 cases					
Parameters	PLC	PLC+BG	PLC+CMBL	PLC+WiggleZ	all combined
$\Omega_b^0 h^2$	$0.0220^{+0.0008}_{-0.001}$	$0.0221^{+0.0007}_{-0.0006}$	$0.0220^{+0.0008}_{-0.0008}$	$0.0226^{+0.0007}_{-0.0007}$	$0.0221^{+0.0007}_{-0.0006}$
$\Omega_c^0 h^2$	$0.119^{+0.009}_{-0.006}$	$0.118^{+0.003}_{-0.003}$	$0.118^{+0.006}_{-0.006}$	$0.130^{+0.007}_{-0.007}$	$0.118^{+0.003}_{-0.003}$
$100\theta_{MC}$	$1.041^{+0.002}_{-0.002}$	$1.041^{+0.001}_{-0.001}$	$1.041^{+0.001}_{-0.001}$	$1.042^{+0.001}_{-0.001}$	$1.041^{+0.001}_{-0.001}$
τ	$0.08^{+0.05}_{-0.03}$	$0.09^{+0.03}_{-0.03}$	$0.08^{+0.04}_{-0.03}$	$0.12^{+0.03}_{-0.03}$	$0.08^{+0.03}_{-0.03}$
n_s	$0.95^{+0.02}_{-0.02}$	$0.96^{+0.01}_{-0.01}$	$0.96^{+0.02}_{-0.02}$	$0.97^{+0.02}_{-0.02}$	$0.96^{+0.01}_{-0.01}$
$\ln(10^{10} A_s)$	$3.08^{+0.08}_{-0.06}$	$3.09^{+0.07}_{-0.06}$	$3.08^{+0.07}_{-0.06}$	$3.15^{+0.07}_{-0.06}$	$3.08^{+0.07}_{-0.06}$
H_0	67^{+3}_{-4}	67^{+1}_{-1}	67^{+3}_{-3}	69^{+3}_{-3}	67^{+1}_{-1}
Ω_m^0	$0.31^{+0.05}_{-0.04}$	$0.30^{+0.02}_{-0.02}$	$0.30^{+0.04}_{-0.03}$	$0.38^{+0.05}_{-0.04}$	$0.30^{+0.02}_{-0.02}$

Table 3: Mean values and 99.7% C.L. bounds on several cosmological parameters. Notice that these bounds do not change for the Λ CDM, H3, and H2 cases.

References

- [1] S. Liberati, “Tests of Lorentz invariance: a 2013 update,” *Class. Quant. Grav.* **30**, 133001 (2013) [arXiv:1304.5795 [gr-qc]].
- [2] A. Silvestri and M. Trodden, “Approaches to Understanding Cosmic Acceleration,” *Rept. Prog. Phys.* **72**, 096901 (2009) [arXiv:0904.0024 [astro-ph.CO]].
- [3] T. Clifton, P. G. Ferreira, A. Padilla and C. Skordis, “Modified Gravity and Cosmology,” *Phys. Rept.* **513**, 1 (2012) [arXiv:1106.2476 [astro-ph.CO]].
- [4] A. Joyce, B. Jain, J. Khoury and M. Trodden, “Beyond the Cosmological Standard Model,” *Phys. Rept.* **568**, 1 (2015) [arXiv:1407.0059 [astro-ph.CO]].
- [5] V. A. Kostelecky and N. Russell, “Data Tables for Lorentz and CPT Violation,” *Rev. Mod. Phys.* **83**, 11 (2011) [arXiv:0801.0287 [hep-ph]].
- [6] D. Colladay and V. A. Kostelecky, “CPT violation and the standard model,” *Phys. Rev. D* **55**, 6760 (1997) [hep-ph/9703464].
- [7] D. Colladay and V. A. Kostelecky, “Lorentz violating extension of the standard model,” *Phys. Rev. D* **58**, 116002 (1998) [hep-ph/9809521].
- [8] C. M. Will, “The Confrontation between General Relativity and Experiment,” *Living Rev. Rel.* **17**, 4 (2014) [arXiv:1403.7377 [gr-qc]].
- [9] K. Yagi, D. Blas, N. Yunes and E. Barausse, “Strong Binary Pulsar Constraints on Lorentz Violation in Gravity,” *Phys. Rev. Lett.* **112**, no. 16, 161101 (2014) [arXiv:1307.6219 [gr-qc]].
- [10] K. Yagi, D. Blas, E. Barausse and N. Yunes, “Constraints on Einstein-theory and Hořava gravity from binary pulsar observations,” *Phys. Rev. D* **89**, no. 8, 084067 (2014) [*Phys. Rev. D* **90**, no. 6, 069902 (2014)] [*Phys. Rev. D* **90**, no. 6, 069901 (2014)] [arXiv:1311.7144 [gr-qc]].

- [11] S. M. Carroll and E. A. Lim, “Lorentz-violating vector fields slow the universe down,” *Phys. Rev. D* **70**, 123525 (2004) [hep-th/0407149].
- [12] J. A. Zuntz, P. G. Ferreira and T. G. Zlosnik, “Constraining Lorentz violation with cosmology,” *Phys. Rev. Lett.* **101**, 261102 (2008) [arXiv:0808.1824 [gr-qc]].
- [13] B. Audren, D. Blas, J. Lesgourgues and S. Sibiryakov, “Cosmological constraints on Lorentz violating dark energy,” *JCAP* **1308**, 039 (2013) [arXiv:1305.0009 [astro-ph.CO]].
- [14] D. Blas, M. M. Ivanov and S. Sibiryakov, “Testing Lorentz invariance of dark matter,” *JCAP* **1210**, 057 (2012) [arXiv:1209.0464 [astro-ph.CO]].
- [15] B. Audren, D. Blas, M. M. Ivanov, J. Lesgourgues and S. Sibiryakov, “Cosmological constraints on deviations from Lorentz invariance in gravity and dark matter,” *JCAP* **1503**, no. 03, 016 (2015) [arXiv:1410.6514 [astro-ph.CO]].
- [16] P. Hořava, “Membranes at Quantum Criticality,” *JHEP* **0903** (2009) 020 [arXiv:0812.4287 [hep-th]].
- [17] P. Hořava, “Quantum Gravity at a Lifshitz Point,” *Phys. Rev. D* **79** (2009) 084008 [arXiv:0901.3775 [hep-th]].
- [18] G. Calcagni, “Cosmology of the Lifshitz universe,” *JHEP* **0909**, 112 (2009) [arXiv:0904.0829 [hep-th]].
- [19] E. Kiritsis and G. Kofinas, “Horava-Lifshitz Cosmology,” *Nucl. Phys. B* **821**, 467 (2009) [arXiv:0904.1334 [hep-th]].
- [20] R. Brandenberger, “Matter Bounce in Horava-Lifshitz Cosmology,” *Phys. Rev. D* **80**, 043516 (2009) [arXiv:0904.2835 [hep-th]].
- [21] S. Mukohyama, “Scale-invariant cosmological perturbations from Horava-Lifshitz gravity without inflation,” *JCAP* **0906**, 001 (2009) [arXiv:0904.2190 [hep-th]].
- [22] R. G. Cai, B. Hu and H. B. Zhang, *Phys. Rev. D* **80**, 041501 (2009) [arXiv:0905.0255 [hep-th]].
- [23] R. G. Cai, B. Hu and H. B. Zhang, *Phys. Rev. D* **83**, 084009 (2011) [arXiv:1008.5048 [hep-th]].
- [24] X. Gao, Y. Wang, R. Brandenberger and A. Riotto, “Cosmological Perturbations in Horava-Lifshitz Gravity,” *Phys. Rev. D* **81**, 083508 (2010) [arXiv:0905.3821 [hep-th]].
- [25] A. Wang and R. Maartens, “Linear perturbations of cosmological models in the Horava-Lifshitz theory of gravity without detailed balance,” *Phys. Rev. D* **81**, 024009 (2010) [arXiv:0907.1748 [hep-th]].
- [26] T. Kobayashi, Y. Urakawa and M. Yamaguchi, “Large scale evolution of the curvature perturbation in Horava-Lifshitz cosmology,” *JCAP* **0911**, 015 (2009) [arXiv:0908.1005 [astro-ph.CO]].
- [27] T. Kobayashi, Y. Urakawa and M. Yamaguchi, “Cosmological perturbations in a healthy extension of Horava gravity,” *JCAP* **1004**, 025 (2010) [arXiv:1002.3101 [hep-th]].
- [28] G. Gubitosi, F. Piazza and F. Vernizzi, “The Effective Field Theory of Dark Energy,” *JCAP* **1302**, 032 (2013) [arXiv:1210.0201 [hep-th]].
- [29] J. K. Bloomfield, É. É. Flanagan, M. Park and S. Watson, “Dark energy or modified gravity? An effective field theory approach,” *JCAP* **1308**, 010 (2013) [arXiv:1211.7054 [astro-ph.CO]].
- [30] J. Gleyzes, D. Langlois, F. Piazza and F. Vernizzi, “Essential Building Blocks of Dark Energy,” *JCAP* **1308**, 025 (2013) [arXiv:1304.4840 [hep-th]].
- [31] J. Bloomfield, “A Simplified Approach to General Scalar-Tensor Theories,” *JCAP* **1312**, 044 (2013) [arXiv:1304.6712 [astro-ph.CO]].
- [32] F. Piazza and F. Vernizzi, “Effective Field Theory of Cosmological Perturbations,” *Class. Quant. Grav.* **30**, 214007 (2013) [arXiv:1307.4350].
- [33] N. Frusciante, M. Raveri and A. Silvestri, “Effective Field Theory of Dark Energy: a Dynamical Analysis,” *JCAP* **1402**, 026 (2014) [arXiv:1310.6026 [astro-ph.CO]].
- [34] J. Gleyzes, D. Langlois and F. Vernizzi, “A unifying description of dark energy,” *Int. J. Mod. Phys. D* **23**, no. 13, 1443010 (2015) [arXiv:1411.3712 [hep-th]].

- [35] C. Cheung, P. Creminelli, A. L. Fitzpatrick, J. Kaplan and L. Senatore, “The Effective Field Theory of Inflation,” *JHEP* **0803**, 014 (2008) [arXiv:0709.0293 [hep-th]].
- [36] S. Weinberg, “Effective Field Theory for Inflation,” *Phys. Rev. D* **77**, 123541 (2008) [arXiv:0804.4291 [hep-th]].
- [37] P. Creminelli, G. D’Amico, J. Norena and F. Vernizzi, “The Effective Theory of Quintessence: the $w_j=1$ Side Unveiled,” *JCAP* **0902**, 018 (2009) [arXiv:0811.0827 [astro-ph]].
- [38] B. Hu, M. Raveri, N. Frusciante and A. Silvestri, “Effective Field Theory of Cosmic Acceleration: an implementation in CAMB,” *Phys. Rev. D* **89**, 103530 (2014) [arXiv:1312.5742 [astro-ph.CO]].
- [39] M. Raveri, B. Hu, N. Frusciante and A. Silvestri, “Effective Field Theory of Cosmic Acceleration: constraining dark energy with CMB data,” *Phys. Rev. D* **90**, 043513 (2014) [arXiv:1405.1022 [astro-ph.CO]].
- [40] B. Hu, M. Raveri, A. Silvestri and N. Frusciante, “EFTCAMB/EFTCosmoMC: massive neutrinos in dark cosmologies,” arXiv:1410.5807 [astro-ph.CO].
- [41] B. Hu, M. Raveri, N. Frusciante and A. Silvestri, “EFTCAMB/EFTCosmoMC: Numerical Notes v1.0,” arXiv:1405.3590 [astro-ph.IM].
- [42] <http://camb.info> .
- [43] A. Lewis, A. Challinor and A. Lasenby, “Efficient computation of CMB anisotropies in closed FRW models,” *Astrophys. J.* **538**, 473 (2000), [astro-ph/9911177].
- [44] A. Lewis and S. Bridle, “Cosmological parameters from CMB and other data: A Monte Carlo approach,” *Phys. Rev. D* **66**, 103511 (2002) [astro-ph/0205436].
- [45] R. Kase and S. Tsujikawa, “Effective field theory approach to modified gravity including Horndeski theory and HoavaLifshitz gravity,” *Int. J. Mod. Phys. D* **23**, no. 13, 1443008 (2015) [arXiv:1409.1984 [hep-th]].
- [46] D. Blas, O. Pujolas and S. Sibiryakov, “Consistent Extension of Horava Gravity,” *Phys. Rev. Lett.* **104** (2010) 181302 [arXiv:0909.3525 [hep-th]].
- [47] M. Ostrogradski, *Mem. Ac. St. Petersburg* **VI 4**, 385 (1850).
- [48] M. Visser, “Lorentz symmetry breaking as a quantum field theory regulator,” *Phys. Rev. D* **80** (2009) 025011 [arXiv:0902.0590 [hep-th]].
- [49] M. Visser, “Power-counting renormalizability of generalized Horava gravity,” arXiv:0912.4757 [hep-th].
- [50] T. P. Sotiriou, M. Visser and S. Weinfurtner, “Phenomenologically viable Lorentz-violating quantum gravity,” *Phys. Rev. Lett.* **102**, 251601 (2009) [arXiv:0904.4464 [hep-th]].
- [51] T. P. Sotiriou, M. Visser and S. Weinfurtner, “Quantum gravity without Lorentz invariance,” *JHEP* **0910**, 033 (2009) [arXiv:0905.2798 [hep-th]].
- [52] T. P. Sotiriou, “Horava-Lifshitz gravity: a status report,” *J. Phys. Conf. Ser.* **283** (2011) 012034 [arXiv:1010.3218 [hep-th]].
- [53] M. Visser, “Status of Horava gravity: A personal perspective,” *J. Phys. Conf. Ser.* **314** (2011) 012002 [arXiv:1103.5587 [hep-th]].
- [54] D. Vernieri and T. P. Sotiriou, “Horava-Lifshitz Gravity: Detailed Balance Revisited,” *Phys. Rev. D* **85** (2012) 064003 [arXiv:1112.3385 [hep-th]].
- [55] D. Vernieri and T. P. Sotiriou, “Hořava-Lifshitz gravity with detailed balance,” *J. Phys. Conf. Ser.* **453** (2013) 012022 [arXiv:1212.4402 [hep-th]].
- [56] D. Vernieri, “On power-counting renormalizability of Hořava gravity with detailed balance,” *Phys. Rev. D* **91**, no. 12, 124029 (2015) [arXiv:1502.06607 [hep-th]].
- [57] E.ourgoulhon, “3+1 formalism and bases of numerical relativity,” gr-qc/0703035 [GR-QC].
- [58] H. Nariai, *Prog. Theor. Phys.* **49**, 165 (1973).

- [59] V. T. Gurovich and A. A. Starobinsky, *Sov. Phys. JETP* **50**, 844 (1979) [*Zh. Eksp. Teor. Fiz.* **77**, 1683 (1979)].
- [60] J. F. Bell, F. Camilo and T. Damour, “A Tighter test of local Lorentz invariance of gravity using PSR-2317+1439,” *Astrophys. J.* **464**, 857 (1996) [astro-ph/9512100].
- [61] D. Blas, O. Pujolas and S. Sibiryakov, “Models of non-relativistic quantum gravity: The Good, the bad and the healthy,” *JHEP* **1104**, 018 (2011) [arXiv:1007.3503 [hep-th]].
- [62] D. Blas and H. Sanctuary, “Gravitational Radiation in Horava Gravity,” *Phys. Rev. D* **84**, 064004 (2011) [arXiv:1105.5149 [gr-qc]].
- [63] M. Bonetti and E. Barausse, “Post-Newtonian constraints on Lorentz-violating gravity theories with a MOND phenomenology,” *Phys. Rev. D* **91**, no. 8, 084053 (2015) [arXiv:1502.05554 [gr-qc]].
- [64] J. W. Elliott, G. D. Moore and H. Stoica, “Constraining the new Aether: Gravitational Cerenkov radiation,” *JHEP* **0508**, 066 (2005) [hep-ph/0505211].
- [65] L. Amendola, R. Gannouji, D. Polarski and S. Tsujikawa, “Conditions for the cosmological viability of $f(R)$ dark energy models,” *Phys. Rev. D* **75**, 083504 (2007) [gr-qc/0612180].
- [66] A. Silvestri, L. Pogosian and R. V. Buniy, “Practical approach to cosmological perturbations in modified gravity,” *Phys. Rev. D* **87**, no. 10, 104015 (2013) [arXiv:1302.1193 [astro-ph.CO]].
- [67] R. K. Sachs and A. M. Wolfe, “Perturbations of a cosmological model and angular variations of the microwave background,” *Astrophys. J.* **147**, 73 (1967) [*Gen. Rel. Grav.* **39**, 1929 (2007)].
- [68] L. Amendola, G. Ballesteros and V. Pettorino, “Effects of modified gravity on B-mode polarization,” *Phys. Rev. D* **90**, 043009 (2014) [arXiv:1405.7004 [astro-ph.CO]].
- [69] M. Raveri, C. Baccigalupi, A. Silvestri and S. Y. Zhou, “Measuring the speed of cosmological gravitational waves,” *Phys. Rev. D* **91**, no. 6, 061501 (2015) [arXiv:1405.7974 [astro-ph.CO]].
- [70] P. A. R. Ade *et al.* [Planck Collaboration], “Planck 2013 results. XV. CMB power spectra and likelihood,” arXiv:1303.5075 [astro-ph.CO].
- [71] P. A. R. Ade *et al.* [Planck Collaboration], “Planck 2013 results. XVI. Cosmological parameters,” *Astron. Astrophys.* (2014) [arXiv:1303.5076 [astro-ph.CO]].
- [72] G. Hinshaw *et al.* [WMAP Collaboration], “Nine-Year Wilkinson Microwave Anisotropy Probe (WMAP) Observations: Cosmological Parameter Results,” *Astrophys. J. Suppl.* **208**, 19 (2013), [arXiv:1212.5226 [astro-ph.CO]].
- [73] A. G. Riess, L. Macri, S. Casertano, H. Lampeitl, H. C. Ferguson, A. V. Filippenko, S. W. Jha and W. Li *et al.*, “A 3% Solution: Determination of the Hubble Constant with the Hubble Space Telescope and Wide Field Camera 3,” *Astrophys. J.* **730**, 119 (2011) [*Astrophys. J.* **732**, 129 (2011)] [arXiv:1103.2976 [astro-ph.CO]].
- [74] M. Betoule *et al.* [SDSS Collaboration], “Improved cosmological constraints from a joint analysis of the SDSS-II and SNLS supernova samples,” *Astron. Astrophys.* **568**, A22 (2014) [arXiv:1401.4064 [astro-ph.CO]].
- [75] A. J. Ross, L. Samushia, C. Howlett, W. J. Percival, A. Burden and M. Manera, “The clustering of the SDSS DR7 main Galaxy sample I. A 4 per cent distance measure at $z = 0.15$,” *Mon. Not. Roy. Astron. Soc.* **449**, no. 1, 835 (2015) [arXiv:1409.3242 [astro-ph.CO]].
- [76] L. Anderson *et al.* [BOSS Collaboration], “The clustering of galaxies in the SDSS-III Baryon Oscillation Spectroscopic Survey: baryon acoustic oscillations in the Data Releases 10 and 11 Galaxy samples,” *Mon. Not. Roy. Astron. Soc.* **441**, no. 1, 24 (2014) [arXiv:1312.4877 [astro-ph.CO]].
- [77] F. Beutler, C. Blake, M. Colless, D. H. Jones, L. Staveley-Smith, L. Campbell, Q. Parker and W. Saunders *et al.*, “The 6dF Galaxy Survey: Baryon Acoustic Oscillations and the Local Hubble Constant,” *Mon. Not. Roy. Astron. Soc.* **416**, 3017 (2011) [arXiv:1106.3366 [astro-ph.CO]].
- [78] P. A. R. Ade *et al.* [Planck Collaboration], “Planck 2013 results. XVII. Gravitational lensing by large-scale structure,” arXiv:1303.5077 [astro-ph.CO].
- [79] <http://smp.uq.edu.au/wigglez-data>

- [80] M. J. Drinkwater *et al.*, “The WiggleZ Dark Energy Survey: Survey Design and First Data Release,” *Mon. Not. Roy. Astron. Soc.* **401**, 1429 (2010) [arXiv:0911.4246 [astro-ph.CO]].
- [81] D. Parkinson *et al.*, “The WiggleZ Dark Energy Survey: Final data release and cosmological results,” *Phys. Rev. D* **86**, 103518 (2012) [arXiv:1210.2130 [astro-ph.CO]].
- [82] C. Blake *et al.*, “The WiggleZ Dark Energy Survey: the selection function and $z=0.6$ galaxy power spectrum,” *Mon. Not. Roy. Astron. Soc.* **406**, 803 (2010) [arXiv:1003.5721 [astro-ph.CO]].
- [83] J. Dossett, B. Hu and D. Parkinson, “Constraining models of $f(R)$ gravity with Planck and WiggleZ power spectrum data,” *JCAP* **1403**, 046 (2014) [arXiv:1401.3980 [astro-ph.CO]].
- [84] P. A. R. Ade *et al.* [Planck Collaboration], “Planck 2015 results. XIII. Cosmological parameters,” arXiv:1502.01589 [astro-ph.CO].
- [85] B. Hu and M. Raveri, “Can modified gravity models reconcile the tension between the CMB anisotropy and lensing maps in Planck-like observations?,” *Phys. Rev. D* **91**, no. 12, 123515 (2015) [arXiv:1502.06599 [astro-ph.CO]].
- [86] N. Frusciante, G. Papadomanolakis, A. Silvestri, *in preparation*